Numerical instabilities of vector invariant momentum equations on rectangular C-grids

Michael J. Bell a and Pedro S. Peixoto bc and John Thuburn b

Sat Oct 22 06:56:47 2016

a Met Office, Fitzroy Rd, Exeter, UK
b College of Engineering, Mathematics and Physical Sciences, University of Exeter, UK
c Instituto de Matemática e Estat stica, Universidade de São Paulo, Brazil
Met Office, Fitzroy Rd, Exeter, EX1 3PB.

Accepted Article

1.3 The linear stability of two well known energy and enstrophy conserving schemes for the vector invariant hydrostatic primitive equations is examined. The problem is analysed for a stably stratified Boussinesq fluid on an f-plane, with a constant velocity field, in height and isopycnal coordinates, by separation of variables into vertical normal modes and a linearised form of the shallow water equations (SWEs). As found by [Hollingsworth ~al.(1983)Hollingsworth, Kallberg, Renner and Burridge], (HKRB hereafter) the schemes are linearly unstable in height coordinate models, due to a non-cancellation of terms in the momentum equations. The schemes with the modified formulations of the kinetic energy proposed by HKRB are shown to have Hermitain stability matrices and hence to be stable to all perturbations. All perturbations in isopycnal models are also shown to be neutrally stable, even with the original formulations for kinetic energy. Analytical expressions are derived for the smallest equivalent depths obtained using Charney-Phillips and Lorenz vertical grids, which show that the Lorenz grid has larger growth rates for the unstable schemes than the Charney-Phillips grid. Test cases are proposed for assessing the stability of new numerical schemes using the SWEs.

Bell, Peixoto and ThuburnNumerical instabilities of vector invariant momentum equations

Hollingsworth instabilities, vector invariant momentum equations, shallow water equations, separation of variables, energy and enstrophy conservation

1 Introduction

The vector invariant form of the momentum equations expresses the advection of momentum as the sum of the gradient of the kinetic energy and the vector product of the velocity and the vorticity. This form is used to derive Kelvin's circulation theorem [Pedlosky(1987)] and was used by [Sadourny(1975)] to discretise the shallow water equations (SWEs). In that paper Sadourny proposed two schemes, demonstrating that one conserves energy and the other, now known as the ens scheme, conserves the volume integral of potential enstrophy (the square of the potential vorticity). He later devised the een (energy and enstrophy) scheme, which for the SWEs conserves the total energy for general flows and enstrophy for non-divergent flows. This scheme was tested in a hydrostatic primitive equation (HPE) model using pressure based sigma coordinates by [Burridge and Haseler(1977)]. [Arakawa and Lamb(1981)], hereafter referred to as AL, derived the Arakawa-Lamb (AL) scheme which, for the SWEs, conserves the total energy

This article has been accepted for publication and undergone full peer review but has not been through the copyediting, typesetting, pagination and proofreading process, which may lead to differences between this version and the Version of Record. Please cite this article as doi: 10.1002/qj.2950

This article is protected by copyright. All rights reserved.

Accepted Article

and enstrophy for general flows. AL also provided a proof of the conservation properties of the een scheme.

[Hollingsworth ~al.(1983)Hollingsworth, Kallberg, Renner and Burridge], HKRB hereafter, reported that the een scheme as implemented by [Burridge and Haseler(1977)] was prone to near-grid-scale instabilities which reduced the kinetic energy of the jet stream particularly in their higher resolution model. They provided an heuristic linear stability analysis which accounted for the 3-grid-point structure of the instabilities in the horizontal and predicted that the growth rates should be proportional to fu/c, where f is the Coriolis parameter, u is the speed of the flow in the basic state and $c = \sqrt{gH}$ is the gravity wave speed. This prediction was consistent with their experimental results for different speeds u and their finding that the modes with highest vertical wavenumber (and smallest speeds c) are the most unstable ones. From the dispersion relationship derived by HKRB it is clear that the instability is a form of destabilised inertia-gravity wave. HKRB also proposed a modified scheme involving reformulations of the kinetic energy gradient and the mass fluxes for the een scheme and showed that it was effective in suppressing the instabilities. A similarly modified form of the AL scheme can also be used (see section 6 of AL) and [LaziÀ~al.(1986)LaziÀ JanjiÀand Mesinger] derived a modified form of the een scheme for the E-grid.

There has recently been renewed interest in these instabilities for two reasons. Firstly some ocean models now use grids which resolve the Rossby radius of deformation very well. Ducousso and le Sommer (personal communication) found that the NEMO model, which uses the een scheme, when configured with a 1 Nautical Mile grid spacing had significantly reduced kinetic energy in the mesoscale flow unless the kinetic energy was reformulated as proposed by HKRB. Secondly a number of researchers such as [NiÀ~al.(2002)NiÀ Gavrilov and ToÀ, [Thuburn(2008)], [Ringler ~al.(2010)Ringler, Thuburn, Klemp and Skamarock], [Skamarock ~al.(2012)Skamarock, Klemp, Duda, Fowler, Park and Ringler] and [Gassmann(2013)] are seeking to develop atmospheric models using meshes with triangular, hexagonal or pentagonal elements employing the vector invariant momentum equations. [Gassmann(2013)] discusses the Hollingsworth instability from an historical perspective and concludes, in agreement with HKRB, that the instability would be more pronounced the less stable the stratification. She also proposes a method for choosing the formulation of the kinetic energy on regular hexagonal grids so as to minimise the size of the term in the momentum equations which lead to the instabilities. [Skamarock ~al.(2012)Skamarock, Klemp, Duda, Fowler, Park and Ringler] show that their scheme is prone to the Hollingsworth instability and use [Gassmann(2013)]'s formulation of the kinetic energy to suppress it.

As noted above, HKRB provided a good initial theoretical analysis of the instability, but their derivation of the dispersion relationship for the instability included the neglect of a term which was only justified by a rather ad hoc argument. Also some aspects of the occurrence of the instability have not been clarified since the work of HKRB. [Arakawa ~al.(1992)Arakawa, Mechoso and Konor] argue that the properties of isentropic coordinates "do not allow room for" the Hollingsworth instabilities. [Arakawa(2000)] notes that the family of consistent energy and enstrophy conserving schemes (including the een and AL schemes) that AL derived generally behave well for the SWEs. He suggests that the Hollingsworth instabilities arise in pressure or sigma coordinates "at least in part" because of the formal application of the schemes in these coordinates in which the layer depth h is replaced by the thickness of model layers despite the fact that the model levels are not material surfaces. This has left developers of new dynamical cores uncertain how to test their schemes using the SWEs. This is very inconvenient for them

This article is protected by copyright. All rights reserved.

Accepted Article

and a better understanding of the occurrence of the instabilities in easily accessible variants of the SWEs is highly desirable.

This paper has two main aims. The first is to confirm that an idealised 3D basic state consisting of a uniform horizontal flow (independent of x, y and z) in a stably stratified fluid on an f-plane can suffer from Hollingsworth instabilities when the original een and AL schemes are used to discretise the equations of motion. Because the isopycnals in the basic state are flat, these linear instabilities can be analysed using separable solutions that are the product of vertically varying normal modes and solutions to linearised SWEs. The resulting linearised SWEs also determine the stability of an appropriately balanced layer of shallow water moving with the same velocity (u_1, v_1) on an f-plane. This result will allow the potential for Hollingsworth instabilities in 3D problems to be explored with new numerical schemes using appropriately specified 2D problems.

The second aim is to derive the matrices determining the dispersion relationships for these linearised SWEs and to analyse them in some detail. It is shown that the modifications proposed by HKRB and AL to the een and AL schemes remove spurious off-diagonal terms (non-cancelling advection terms) from the stability matrix and recover its Hermitian form. This makes the schemes stable for any linear disturbance to the idealised basic states. The original een and AL schemes in isopycnal coordinates are also shown to be neutrally stable to all perturbations. Numerical results and an expression for the instabilities in height coordinates suggest that the most unstable perturbations are fairly closely aligned with the grid.

It is more natural to consider the simple 3D basic state described above in an oceanic context, where variations in the surface height of the ocean can easily occur and affect the pressures at all depths, than in an atmospheric context. For this reason the analysis is presented using the Boussinesq, equations which are appropriate for the ocean (rather than the equations of state for a perfect gas appropriate for the atmosphere). The normal modes of the continuous equations for an atmosphere on a sphere are also separable (provided one makes use of traditional assumptions such as the shallow atmosphere approximation) and the equivalent depth of the vertical modes is independent of their frequency if the motions are taken to be hydrostatic [Daley(1988)]. These points also hold for the vertically discrete equations studied by [Thuburn and Woollings(2005)]. So we would expect our analysis to be relevant to atmosphere models as well as ocean models.

The linear stability analysis of the states described in this paper is most safely approached by writing out the full non-linear governing equations and the description of the basic state in discretised form, then deriving from these the linearised equations, and finally deriving the separable solutions. This approach is unnecessarily lengthy and with some care it is possible to linearise the equations and derive the separable solutions using the continuous equations and then discretise. Section 2 writes down the full non-linear governing equations and the linearised equations for their separable solutions firstly for z-coordinates and secondly for isopycnal coordinates. The derivations of these equations are given in appendices 8 and 9. The linearised equations for the solutions which vary in time and in the horizontal are then derived by linearising two sets of SWEs. The only difference between the two sets of SWEs is that the generalised Coriolis terms in the one relating to isopycnal coordinates are the product of the potential vorticity, q, and a depth weighted velocity $\mathbf{u}^*$, whilst those for height coordinates are the product of the vertical component of the vorticity, Z, and the velocity $\mathbf{u}$. It transpires that this difference is of crucial importance.

Section 3 derives the vertical discretisation of the modes in isopycnal and height

This article is protected by copyright. All rights reserved.

Accepted Article

coordinates. The vertical modes with the highest vertical wavenumbers have small equivalent depths as one would expect from the vertical modes for the continuous problem. It is shown that on the Lorenz grid the smallest equivalent depths reduce as the number of vertical levels (K) increases at a rate which is a factor of K^2 faster than that of the continous modes and that this result is related to the presence of the computational mode on the Lorenz grid. The resulting reduction in the phase speed of the gravity waves (c) on the Lorenz grid for these modes increases their Froude number (F_u) and exacerbates the Hollingsworth instabilities.

Section 4 first describes the discretisation of the SWEs using the een scheme and derives the discrete form of the linearised SWEs for both height and isopycnal coordinates. It then reduces the analysis of the stability of the scheme to an eigenvalue problem involving 3 by 3 matrices written in a non-dimensional form and shows that for the modified form of the een scheme the matrices are Hermitian and hence that the scheme is stable. Section 4 also shows that all linear perturbations are neutrally stable for the original een scheme in isopycnal coordinates. Appendix 11 shows that the same conclusions hold for the AL scheme and appendix 12 provides an interpretation of the stability of the schemes in isopycnal coordinates. Section 4 ends by illustrating the dependence on the Froude and Rossby numbers of the instabilities with the aid of analytical calculations for some special cases and numerical evaluations.

Section 5 illustrates the nature of the instabilities further using integrations of the SWEs and proposes test cases with doubly-periodic Cartesian domains that could be used to test whether new numerical schemes suffer from these instabilities. Section 6 provides a concluding summary and discussion and the tables in appendix 7 provide a summary of the symbols used in the main body of the paper.

2 Model formulation and separation of variables

The governing equations will be taken to be a form of the hydrostatic, incompressible, adiabatic, Boussinesq equations suitable for a liquid. They will be written in Cartesian coordinates and the Coriolis parameter f will be taken to have a constant value f_0. The horizontal kinetic energy per unit mass will be denoted by

$$K_e = \frac{1}{2}(u^2 + v^2), \tag{1}$$

the vertical component of the relative and total vorticities will be denoted by ζ and Z respectively with

$$\zeta = \frac{\partial v}{\partial x} - \frac{\partial u}{\partial y}, \quad Z = f_0 + \zeta, \tag{2}$$

and ρ_{00} will denote a constant density.

2.1 Formulation in height coordinates

Governing equations

In height coordinates, the Bernoulli function Φ is given by

$$\Phi = p/\rho_{00} + K_e, \tag{3}$$

This article is protected by copyright. All rights reserved.

Accepted Article

where p is the pressure field which is in hydrostatic balance with the density ρ and gravity g,

$$\frac{\partial p}{\partial z} = -\rho g. \tag{4}$$

The horizontal momentum equations in vector invariant form are then

$$\begin{aligned} \frac{\partial u}{\partial t} - Zv + w\frac{\partial u}{\partial z} &= -\frac{\partial \Phi}{\partial x} + A_m D_m u, \\ \frac{\partial v}{\partial t} + Zu + w\frac{\partial v}{\partial z} &= -\frac{\partial \Phi}{\partial y} + A_m D_m v. \end{aligned} \tag{5}$$

where w is the vertical velocity, A_m is a coefficient of viscosity, and D_m is a diffusive operator such as ∇_H^2 or $\partial^2/\partial z^2$. The viscosity will be set to zero except in this section and section 4.6 where the stabilising effect of viscous terms on perturbations with small Froude numbers is discussed.

The density, ρ, will be taken to be conserved following the motion,

$$\frac{D\rho}{Dt} = 0, \quad \frac{D}{Dt} = \frac{\partial}{\partial t} + u\frac{\partial}{\partial x} + v\frac{\partial}{\partial y} + w\frac{\partial}{\partial z}, \tag{6}$$

and the flow will be assumed to be incompressible

$$\frac{\partial u}{\partial x} + \frac{\partial v}{\partial y} + \frac{\partial w}{\partial z} = 0. \tag{7}$$

The domain will be taken to be unbounded in x and y and to have a flat boundary at $z = -H$ where the vertical velocity is zero. Attention will be focussed solely on the baroclinic modes for which to a very good approximation the upper boundary at $z = 0$ also has zero normal velocity so

$$w = 0, \quad z = 0, -H. \tag{8}$$

The barotropic mode satisfies the shallow water equations (to a very good approximation) and is not considered further in this section.

Separable solutions to the linearised equations

The evolution of very small amplitude perturbations can be determined by linearising the hydrostatic Boussinesq equations about a basic state.

The assumed basic state consists of a stably stratified density field $\rho_0(z)$, that is in hydrostatic balance with the pressure field $p_0(z)$, and a horizontal velocity field with components $u = u_1$ and $v = v_1$ which does not depend on x, y, z or t. This velocity field is in geostrophic balance with a pressure field p_1 which is independent of z, and the vertical velocity w_0 is zero. The non-zero velocity in the basic state and the non-linearities in the equations of motions give the potential for instabilities.

These linearised equations enjoy separable solutions. The derivation is detailed in Appendix 8, which is a straightforward generalisation of section 6.11 of [Gill(1982)]. Denoting the small amplitude perturbations by primed variables, functions varying only in the horizontal and time by tildes and functions varying only in the vertical by hats, the horizontal velocity and pressure pertubations are expressed in the forms:

This article is protected by copyright. All rights reserved.

Accepted Article

$$\begin{aligned} u' &= \tilde{u}(x,y,t)\frac{\hat{p}(z)}{g\rho_{00}}, \quad v' = \tilde{v}(x,y,t)\frac{\hat{p}(z)}{g\rho_{00}}, \\ p' &= \tilde{\eta}(x,y,t)\hat{p}(z). \end{aligned} \tag{9}$$

The solutions dependent only on x, y and t are determined by the linearised horizontal momentum equations,

$$\begin{aligned} \frac{\partial \tilde{u}}{\partial t} - f_0\tilde{v} - \tilde{\zeta}v_1 &= -\frac{\partial \tilde{\Phi}}{\partial x} + A_m D_m \tilde{u}, \\ \frac{\partial \tilde{v}}{\partial t} + f_0\tilde{u} + \tilde{\zeta}u_1 &= -\frac{\partial \tilde{\Phi}}{\partial y} + A_m D_m \tilde{v}, \end{aligned} \tag{10}$$

where

$$\tilde{\Phi}(x,y,t) = g\tilde{\eta} + u_1\tilde{u} + v_1\tilde{v}, \tag{11}$$

and a continuity equation

$$\frac{\partial \tilde{\eta}}{\partial t} + u_1\frac{\partial \tilde{\eta}}{\partial x} + v_1\frac{\partial \tilde{\eta}}{\partial y} + H_e\left(\frac{\partial \tilde{u}}{\partial x} + \frac{\partial \tilde{v}}{\partial y}\right) = 0, \tag{12}$$

where H_e is the equivalent depth (a separation constant). This system is the linearised form of a shallow water system (see below).

The vertical structure of the perturbed variables is given by

$$\frac{\mathrm{d}\hat{p}}{\mathrm{d}z} = -g\hat{\rho}, \tag{13}$$

$$H_e\hat{\rho} = -\frac{\mathrm{d}\rho_0}{\mathrm{d}z}\hat{h}, \tag{14}$$

$$\frac{\hat{p}}{g\rho_{00}} = \frac{\mathrm{d}\hat{h}}{\mathrm{d}z}, \tag{15}$$

where $\hat{\rho}(z)$ and $\hat{h}(z)$ describe the vertical variation of the perturbation's density and vertical velocity fields. The boundary conditions are given by

$$\hat{h} = 0, \quad z = 0, -H. \tag{16}$$

2.2 Formulation in isopycnal coordinates

Governing equations

Following section 3.9.1 of [Vallis(2006)] we write the density and pressure fields in the form

$$\rho = \rho_{00} + \delta\rho, \quad p = p_0(z) + \delta p, \tag{17}$$

This article is protected by copyright. All rights reserved.

Accepted Article

$$\frac{\mathrm{d}p_0}{\mathrm{d}z} = -g\rho_{00}. \tag{18}$$

The buoyancy and an inverse measure of the stratification for this system are then given by

$$b = -\frac{g\delta\rho}{\rho_{00}}, \quad \sigma = \frac{\partial z}{\partial b}. \tag{19}$$

If the isopycnal coordinates were used in a layer model, σ would represent the thickness of the layers. The Montgomery potential and Bernoulli function are given by

$$M = \frac{\delta p}{\rho_{00}} - bz, \quad \Phi = M + K_e. \tag{20}$$

The horizontal momentum equations are then given by

$$\begin{aligned} \frac{\partial u}{\partial t} - qv^* &= -\frac{\partial \Phi}{\partial x}, \\ \frac{\partial v}{\partial t} + qu^* &= -\frac{\partial \Phi}{\partial y}. \end{aligned} \tag{21}$$

where

$$q = Z/\sigma^{(q)}, \quad u^* = \sigma^{(u)}u, \quad v^* = \sigma^{(v)}v. \tag{22}$$

Here q is the potential vorticity, u^* and v^* are proportional to the fluxes within the layers (i.e. the velocities multiplied by the thicknesses of the layers), and the superscripts (q), (u) and (v) indicate the location at which σ is calculated. They have been included at this stage so that the discretised form of the linearised equations can be inferred easily in section 4.1. As usual the partial derivatives in the momentum equations are evaluated with b held constant and the diapycnal velocities have been set to zero.

The hydrostatic equation then takes the form

$$\frac{\partial M}{\partial b} = -z, \tag{23}$$

and for an ideal Boussinesq fluid the continuity equation is given by

$$\frac{\mathrm{D}\sigma}{\mathrm{D}t} = \frac{\partial \sigma}{\partial t} + u\frac{\partial \sigma}{\partial x} + v\frac{\partial \sigma}{\partial y} = -\sigma\left(\frac{\partial u}{\partial x} + \frac{\partial v}{\partial y}\right), \tag{24}$$

in which all partial derivatives are again evaluated with b held constant.

Denoting the buoyancy at $z = 0$ and $z = -H$ by $b(z = 0) = b(0)$ and $b(z = -H) = b(-H)$ respectively, the boundary conditions of no normal flow are given by

$$\frac{\mathrm{D}z}{\mathrm{D}t} = 0, \quad b = b(0), b(-H). \tag{25}$$

Separable solutions to the linearised equations

Assuming an analogous basic state to that of the height coordinates model, the separable solutions which depend only on x, y and t in a *continuous* model satisfy equations of the same form as those for the height coordinate. However, in a *numerical* isopycnal model extra terms arise because the layer thicknesses (σ) in (22) are calculated at different points. Appendix 9

This article is protected by copyright. All rights reserved.

Accepted Article

shows that the separable solutions which depend on x, y and t satisfy the following horizontal momentum equations

$$\begin{aligned} \frac{\partial \tilde{u}}{\partial t} - f_0 \tilde{v} - \tilde{\zeta} v_1 - \frac{f_0 v_1}{H_e}\left(\tilde{\eta}^{(v)} - \tilde{\eta}^{(q)}\right) &= -\frac{\partial \tilde{\Phi}}{\partial x}, \\ \frac{\partial \tilde{v}}{\partial t} + f_0 \tilde{u} + \tilde{\zeta} u_1 + \frac{f_0 u_1}{H_e}\left(\tilde{\eta}^{(u)} - \tilde{\eta}^{(q)}\right) &= -\frac{\partial \tilde{\Phi}}{\partial y}, \end{aligned} \tag{26}$$

In the horizontally discreted form of (26a) the terms $\tilde{\eta}^{(v)}$ and $\tilde{\eta}^{(q)}$ orginate from different points. They consequently represent different averages of η and their difference is non-zero. The separable solutions also satisfy the continuity equation (12) which is the same as that for the height coordinate model.

Appendix 9 also shows that the vertical structure of the separable solutions is given by

$$g\frac{\mathrm{d}\hat{M}}{\mathrm{d}b} = -\hat{h}, \tag{27}$$

$$H_e \frac{\mathrm{d}\hat{h}}{\mathrm{d}b} = \sigma_0 \hat{M}, \tag{28}$$

where $\hat{h}$ describes the vertical variation in the height z' of the perturbations to the isopycnals and H_e is again the separation constant. The boundary conditions are given by

$$\hat{h} = 0, \quad b = b(0), b(-H). \tag{29}$$

2.3 Formulation for shallow water

The shallow water equations, for a layer of constant density in which the bottom of the fluid is at height z_b and the depth of the fluid layer is η, are given by

$$\begin{aligned} &\frac{\partial u}{\partial t} - Zv = -\frac{\partial \Phi}{\partial x}, \\ &\frac{\partial v}{\partial t} + Zu = -\frac{\partial \Phi}{\partial y}, \\ &\frac{\partial \eta}{\partial t} + \frac{\partial}{\partial x}(\eta u) + \frac{\partial}{\partial y}(\eta v) = 0, \end{aligned} \tag{30}$$

where the Bernoulli potential is given by

$$\Phi = g(\eta + z_b) + K_e. \tag{31}$$

A steady basic state with a constant horizontal velocity field (u_1, v_1) and fluid depth, H_e, which is independent of position, is obtained provided the bathymetry, z_b, is given by

$$g z_b = g z_{b0} + f_0(v_1 x - u_1 y), \tag{32}$$

where b_0 is a constant.

Writing $u' = u - u_1 = \tilde{u}$, $v' = v - v_1 = \tilde{v}$, and $\eta' = \eta - H_e = \tilde{\eta}$ and linearising (30) about this basic state one obtains the equations (10) and (12) derived for height coordinates.

This article is protected by copyright. All rights reserved.

Accepted Article

If one defines

$$q = \frac{Z}{\eta}, \quad u^* = \eta^{(u)} u, \quad v^* = \eta^{(v)} v, \tag{33}$$

replaces Zv by qv^* and Zu by qu^* in (30) and linearises about the same basic state, one obtains the equations (26) and (12) derived for isopycnal coordinates.

A second way to obtain a steady basic state with a fluid depth independent of position is to use a fictitious force added to the momentum equations. One of the numerical test cases in section 5 uses a fictitious force and the other uses a sloping bathymetry to balance the zonal flow.

3 Analysis of the discrete vertical modes

3.1 Discretization in height coordinates

The natural discretisation in the vertical of the level model is not clear cut and it is well known that there are a number of options; see [Tokioka(1978)], [Thuburn and Woollings(2005)] and [Girard ~al.(2014)Girard, Plante, Desgagnà McTaggart-Cowan, Cotà Charron, Gravel, Lee, Patoine, Qaddouri, Roch, Spacek, Tanguay, Vaillancourt and Zadra]. Most ocean models use the Lorenz grid illustrated in Figure 1a in which u, v, p and ρ are stored on full levels and w (and therefore $\hat{h}$) is stored at half-levels. The vertical structure equations (13) - (15) are then discretised as

$$\hat{p}_{k+1} - \hat{p}_k = -\frac{g}{2}\left(\hat{\rho}_{k+1} + \hat{\rho}_k\right)(\Delta z)_{k+1/2}, \tag{34}$$

$$H_e \hat{\rho}_k = -\frac{\mathrm{d}\rho_0}{\mathrm{d}z}\frac{1}{2}\left(\hat{h}_{k+1/2} + \hat{h}_{k-1/2}\right), \tag{35}$$

$$\hat{p}_k (\Delta z)_k = g\rho_{00}\left(\hat{h}_{k+1/2} - \hat{h}_{k-1/2}\right), \tag{36}$$

and the boundary conditions (16) as

$$\hat{h}_{1/2} = \hat{h}_{K+1/2} = 0. \tag{37}$$

Figure 1: The arrangement of variables using (a) height coordinates and (b) isopycnal coordinates. In both grids u and v are held at full levels, and the upper and lower boundaries are at half-levels.

This article is protected by copyright. All rights reserved.

Accepted Article

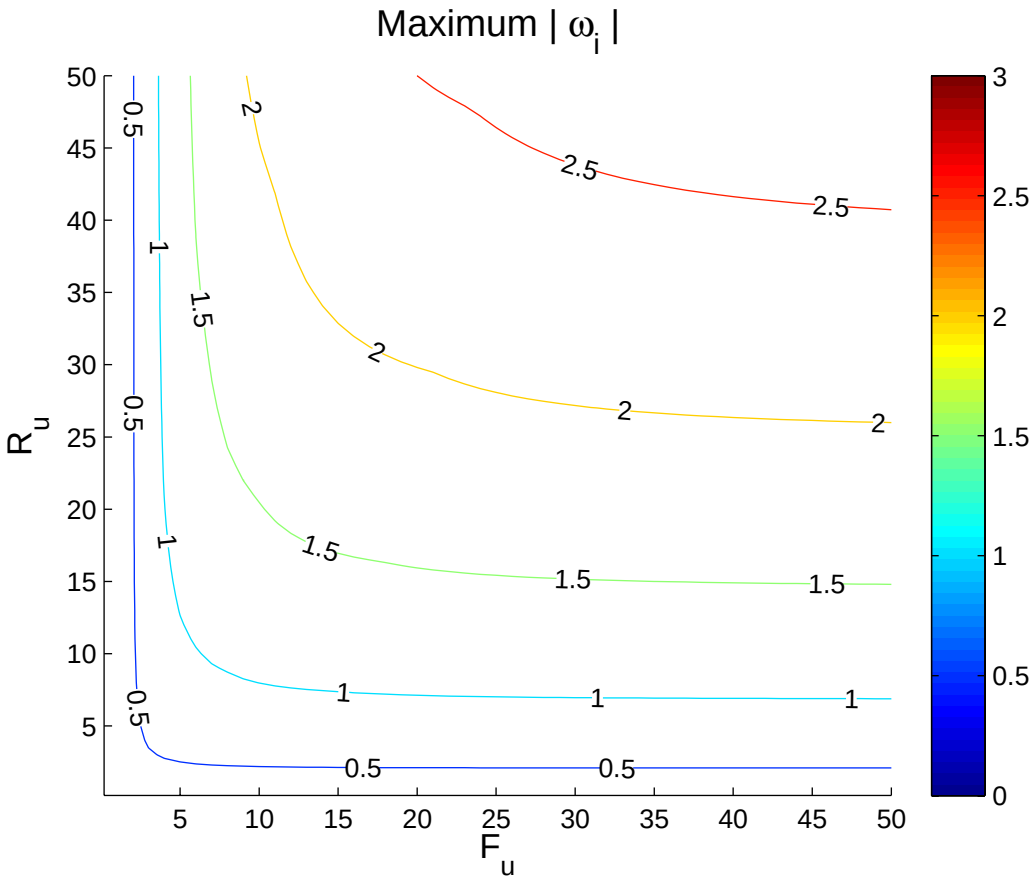

3.2 Discretization in isopycnal coordinates

The natural discretisation in the vertical of the isopycnal model is to take the horizontal boundaries to lie at half levels and to store u, v and M at full levels and z (and therefore $\hat{h}$) at half levels as in Figure 1b. Denoting the levels with a subscript k, the level number increasing with height, (27) and (28) are discretised as

$$g(\hat{M}_{k+1} - \hat{M}_k) = -\hat{h}_{k+1/2}(\Delta b)_{k+1/2}, \tag{38}$$

$$H_e(\hat{h}_{k+1/2} - \hat{h}_{k-1/2}) = \sigma_{0k}\hat{M}_k(\Delta b)_k. \tag{39}$$

For a grid with K levels, the boundary conditions (29) are simply

$$\hat{h}_{1/2} = \hat{h}_{K+1/2} = 0. \tag{40}$$

One sees that (36) and (37) correspond to (39) and (40). Equations (34) and (35) when combined correspond to (38), but in a form that involves more vertical averaging. The discretisation used above for the isopycnal model corresponds to that for the best category in [Thuburn and Woollings(2005)] obtained using a Charney-Phillips grid with potential temperature evaluated at half-levels .

3.3 Discretised vertical modes

This article is protected by copyright. All rights reserved.

Accepted Article

The impact of the vertical discretisation on the equivalent depth, H_e, which is the separation constant and the eigenvalue for the normal modes in the vertical, can be illustrated for the case of uniform stratification and grid-spacing. Then the vertical structure equations for height coordinates (34) - (36) reduce to a single equation

$$\hat{h}_{k+3/2} - 2\Lambda\hat{h}_{k+1/2} + \hat{h}_{k-1/2} = 0, \tag{41}$$

with

$$\begin{aligned} \Lambda &\equiv \frac{4-n^2}{4+n^2}, \\ n^2 &\equiv -\frac{g}{\rho_{00}}\frac{\mathrm{d}\rho_e}{\mathrm{dz}}\frac{\Delta z^2}{gH_e} \approx \frac{\Delta z \Delta b}{gH_e}. \end{aligned} \tag{42}$$

Together with its boundary conditions (41) defines an eigenvalue problem for Λ. These eigenvalues determine n^2 and then H_e through (42).

Similarly (38) and (39) for isopycnal coordinates reduce to (41) with

$$\Lambda \equiv 1 - m^2/2, \quad m^2 = \frac{\sigma_0(\Delta b)^2}{gH_e} = \frac{\Delta z \Delta b}{gH_e}. \tag{43}$$

The last identity above follows from (19b).

The solutions of (41) are given by

$$\hat{h}_{k+1/2} = \mathrm{Re}\{CW^k\}, \quad W = \Lambda \pm \mathrm{i}\sqrt{1-\Lambda^2}. \tag{44}$$

W lies on the unit circle when $-1 \le \Lambda \le 1$ and hence can also be written in the form $W = \exp \mathrm{i}\theta$, where θ is a real argument. The solutions written in this form that also satisfy the boundary conditions, (40) for isopycnal coordinates or (37) for height coordinates, are given by

$$\hat{h}_{k+1/2} = C\sin(\theta k), \quad \theta = \frac{N\pi}{K}, \tag{45}$$

where N is an integer and $1 \le N \le K$.

The solution (45) with $N = K$ has $\hat{h}_{k+1/2} = 0$ for all integer k within the domain so its vertical velocities are zero. From (36) it also has $\hat{p}_k = 0$ for all points in the domain and hence by (9) zero horizontal velocities. When $H_e = 0$, (35) does not constrain $\hat{\rho}$ and (34) is satisfied provided $\hat{\rho}_k = -\hat{\rho}_{k+1}$ at all points in the domain. Hence (45) with $N = K$ corresponds to the computational mode on the Lorenz grid.

The solutions with $N = K - 1$ are the ones with the smallest equivalent depths that can give rise to Hollingsworth instabilities. We now calculate their equivalent depths for the realistic case with $K >> 1$. For these modes

$$W \approx -1 + \frac{\mathrm{i}\pi}{K}. \tag{46}$$

Equating (44b) and (46) one infers that

$$\sqrt{1-\Lambda^2} \approx \frac{\pi}{K}. \tag{47}$$

As Λ is close to -1, one can take $1 - \Lambda^2 = (1-\Lambda)(1+\Lambda) \approx 2(1+\Lambda)$ and infer from (47) that

$$\Lambda \approx -1 + \frac{\pi^2}{2K^2}. \tag{48}$$

This article is protected by copyright. All rights reserved.

Accepted Article

Using (42) and (43) in (48) one finds that for height and isopycnal coordinates respectively

$$n^2 \approx \frac{16K^2}{\pi^2} \quad \text{and} \quad m^2 = 2(1-\Lambda) \approx 4. \tag{49}$$

By (42b) and (43b) the equivalent depth, H_e, is proportional to m^{-2} and also to n^{-2}. For the Charney-Phillips grid (and the continuous equations), H_e is inversely proportional to the square of the vertical wavenumber. If one chooses g so that $H_e = 1000\,\text{m}$ for the first baroclinic mode then for the largest vertical wavenumber on the Charney-Phillips grid, $H_e = 1000K^{-2}\,\text{m}$. For a grid with 100 vertical levels this gives $H_e = 0.1\,\text{m}$ for the most rapidly varying mode. For height coordinates using the Lorenz grid, (49) shows that H_e for the most rapidly varying mode is a factor of $\frac{1}{4}\pi^2 K^{-2}$ smaller which means that it is $2.5\times10^{-4}\,\text{m}$ in the above example.

The solutions above are consistent with those derived by [Tokioka(1978)]. It is however clearer from the analysis above than that of [Tokioka(1978)] that the solutions satisfying (47) have the fastest vertical variation and smallest equivalent depths of all the vertical modes that need to be considered on the Charney-Phillips and Lorenz grids. So all the vertical modes on the Charney-Phillips grid are well-behaved and have equivalent depths of the same order of magnitude as the continuous equations, whilst the modes with the most rapid variation in the vertical on Lorenz grids have much smaller equivalent depths because of their similarity to the computational mode.

4 Analysis of the discretised SWEs

4.1 Formulation of een scheme

For simplicity the equations will be written in Cartesian coordinates and discretised on a C-grid with uniform, but not necessarily isotropic, grid spacing. The arrangement of variables on the C-grid is illustrated in Figure 2.

Figure 2: The staggering of variables on the C-grid. This figure and the indexing is based on [Arakawa and Lamb(1981)].

This article is protected by copyright. All rights reserved.

Accepted Article

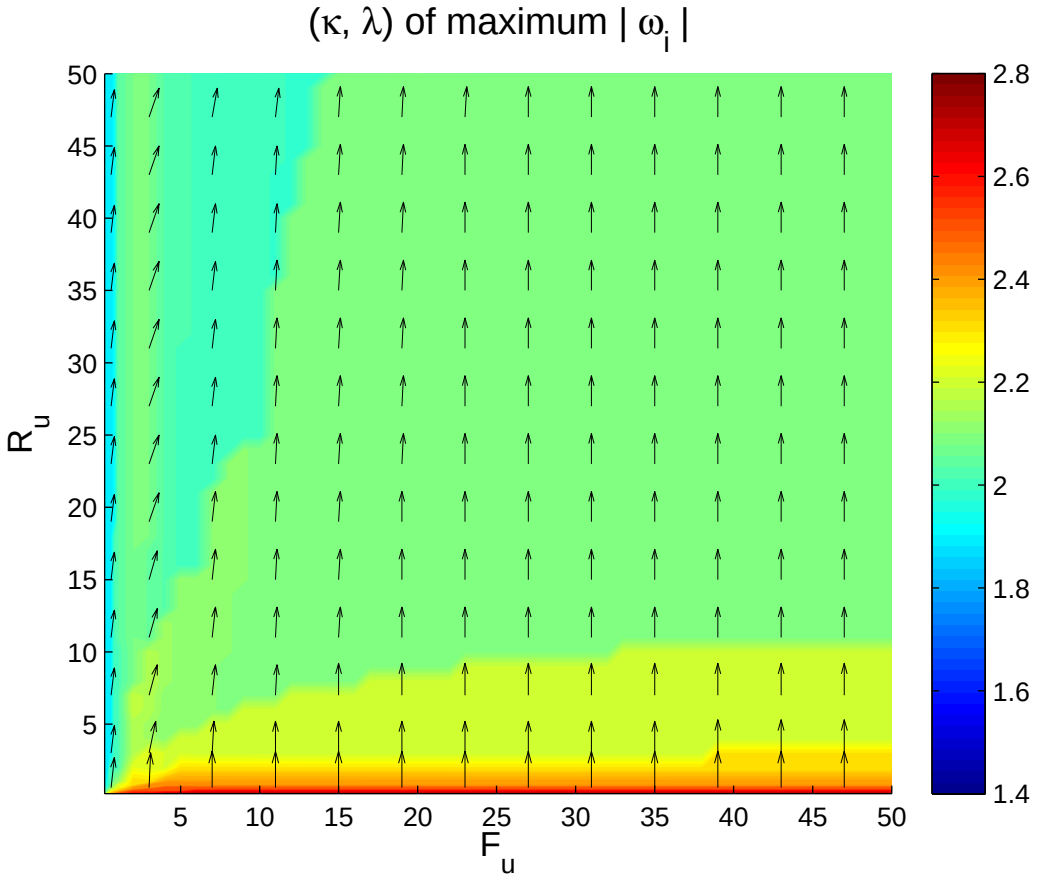

The following difference and average operators will be used. Let ξ denote any of the coordinate directions x, y and z, $\imath$ denote its discrete indexing and ψ denote any function of ξ. Then

$$\begin{aligned} \overline{\psi}^{\xi}_{\imath} &\equiv \frac{1}{2}(\psi_{\imath-1/2}+\psi_{\imath+1/2}), \quad (\Delta\xi)_{\imath} \equiv \xi_{\imath+1/2}-\xi_{\imath-1/2}, \\ (\delta_{\xi}\psi)_{\imath} &\equiv \frac{(\psi_{\imath+1/2}-\psi_{\imath-1/2})}{(\Delta\xi)_{\imath}}, \quad (\delta_{\imath}\psi)_{\imath} \equiv (\Delta\xi)_{\imath}(\delta_{\xi}\psi)_{\imath}. \end{aligned} \tag{50}$$

The index for which the quantity is calculated is usually suppressed. All of these operators commute with each other and obey the associative laws of arithmetic. [Adcroft ~al.(1997)Adcroft, Hill and Marshall] provide a useful summary of identities they satisfy.

The discretisation on a C-grid of ζ as defined by (2a) is given by

$$\zeta = \delta_x v - \delta_y u \tag{51}$$

and the discretisation of the x- and y-derivatives of the Bernoulli function is given by $\delta_x\Phi$ and $\delta_y\Phi$ respectively.

The averaging operators needed to define the modified een scheme are given by

$$\overline{\psi}^{\mu_E} \equiv \frac{1}{3}\psi + \frac{2}{3}\overline{\psi}^{xx}, \quad \overline{\psi}^{\nu_E} \equiv \frac{1}{3}\psi + \frac{2}{3}\overline{\psi}^{yy}, \tag{52}$$

where the E subscript indicates the expression is relevant to the een scheme. Additional

This article is protected by copyright. All rights reserved.

Accepted Article

averaging operators μ_F and ν_F which allow the original and modified schemes to be concisely defined are given by

$$\begin{aligned} \overline{\psi}^{\mu_F} &\equiv \overline{\psi}^{\mu_E}, \quad \overline{\psi}^{\nu_F} \equiv \overline{\psi}^{\nu_E} \text{ (modifiedscheme)}, \\ \overline{\psi}^{\mu_F} &\equiv \psi, \quad \overline{\psi}^{\nu_F} \equiv \psi \quad \text{(originalscheme)}. \end{aligned} \tag{53}$$

For shallow water and isopycnal coordinate models the een scheme calculates (22) using

$$\eta^{(q)} = \overline{\eta}^{xy}, \quad \eta^{(v)} = \overline{\eta}^{y\mu_F}, \qquad \eta^{(u)} = \overline{\eta}^{x\nu_F}. \tag{54}$$

As noted by HKRB, this averaging of the layers also needs to be used in the discretisation of the mass fluxes in the continuity equation,

$$\frac{\partial \eta}{\partial t} + \delta_x\left(\overline{\eta}^{x\nu_F} u\right) + \delta_y\left(\overline{\eta}^{y\mu_F} v\right) = 0, \tag{55}$$

to ensure conservation of total (kinetic plus potential) energy with the modified form of the kinetic energy,

$$2K_E = \overline{u^2}^{x\nu_F} + \overline{v^2}^{y\mu_F}. \tag{56}$$

The een scheme for the SWEs associated with height coordinates discretises the terms Zv and Zu of (30) using

$$\begin{aligned} (Zv)_E &= \frac{2}{3}\overline{(\overline{Z}^{x} v)}^{xy} + \frac{2}{3}\left(\overline{Z}^{y-xy}\right) - \frac{1}{3}\left(\overline{Zv}^{-x}\right)^{y}, \\ (Zu)_E &= \frac{2}{3}\overline{(\overline{Z}^{y} u)}^{xy} + \frac{2}{3}\left(\overline{Z}^{x-xy}\right) - \frac{1}{3}\left(\overline{Zu}^{-y}\right)^{x}. \end{aligned} \tag{57}$$

Expressions for the SWEs associated with isopycnal coordinates are obtained by replacing Z, u and v by q, u^* and v^* respectively in (57). These expressions were noted in HKRB and are briefly derived from the expression for the een scheme used by AL in Appendix 10.

4.2 Linearisation of the een scheme

Using $\delta_x\psi^2 = 2\overline{\psi}^{x}\delta_x\psi$ one finds that the linearised kinetic energy gradient in the x- and y-directions for (56) is given by

$$\begin{aligned} \delta_x K'_E &= u_1\delta_x\overline{u'}^{x\nu_F} + v_1\delta_x\overline{v'}^{y\mu_F}, \\ \delta_y K'_E &= u_1\delta_y\overline{u'}^{x\nu_F} + v_1\delta_y\overline{v'}^{y\mu_F}. \end{aligned} \tag{58}$$

Introducing

$$\delta_I = 0 \quad \text{forheightcoordinates,} 1 \quad \text{forisopycnalcoordinates.} \tag{59}$$

in order to allow the expressions for height and isopycnal coordinates to be combined, linearising (57) one obtains

This article is protected by copyright. All rights reserved.

Accepted Article

$$
\begin{aligned}
(Zv)'_E &= f_0 \overline{v'}^{xy} + \overline{\zeta'}^{y\mu_E} v_1 + \delta_I \frac{f_0 v_1}{H} \left(\overline{\eta'}^{\mu_F} - \overline{\eta'}^{\mu_E} \right)^{xyy}, \\
(Zu)'_E &= f_0 \overline{u'}^{xy} + \overline{\zeta'}^{x\nu_E} u_1 + \delta_I \frac{f_0 u_1}{H} \left(\overline{\eta'}^{\nu_F} - \overline{\eta'}^{\nu_E} \right)^{xxy},
\end{aligned}
\tag{60}
$$

Using (51) in (58) and (60), one sees that the discrete linearised form of the momentum SWE (30) is given by

$$
\begin{aligned}
&\frac{\partial u'}{\partial t} - f_0 \overline{v'}^{xy} + g \delta_x \eta' + u_1 \delta_x \overline{u'}^{x\nu_F} + v_1 \delta_y \overline{u'}^{y\mu_E} \quad + \\
&v_1 \delta_x \left(\overline{v'}^{y\mu_F} - \overline{v'}^{y\mu_E} \right) - \delta_I \frac{f_0 v_1}{H} \left(\overline{\eta'}^{\mu_F} - \overline{\eta'}^{\mu_E} \right)^{xyy} \quad = 0, \\
&\frac{\partial v'}{\partial t} + f_0 \overline{u'}^{xy} + g \delta_y \eta' + u_1 \delta_x \overline{v'}^{x\nu_E} + v_1 \delta_y \overline{v'}^{y\mu_F} \quad + \\
&u_1 \delta_y \left(\overline{u'}^{x\nu_F} - \overline{u'}^{x\nu_E} \right) + \delta_I \frac{f_0 u_1}{H} \left(\overline{\eta'}^{\nu_F} - \overline{\eta'}^{\nu_E} \right)^{xxy} \quad = 0,
\end{aligned}
\tag{61}
$$

The first line of each equation above consists of terms corresponding to those present in the continuous equations. The second line consists of additional terms arising from the discretisation employed which have the potential to give rise to spurious effects (the non-cancelling terms of HKRB). In HKRB the basic flow was taken to be zonal, $v_1 = 0$, and the terms proportional to δ_I were not considered. The instability of the original scheme was traced by HKRB to lack of cancellation between $\overline{u'}^{x\nu_F} = \overline{u'}^{x}$ and $\overline{u'}^{x\nu_E}$ in the first term on the second line of the y-component of the momentum equation. The kinetic energy in their modified scheme was re-formulated as in (56) to ensure that this term is identically zero ($\overline{u'}^{x\nu_F} = \overline{u'}^{x\nu_E}$).

Both terms on the second line of each of the equations in (61) are zero for the modified schemes in both height and isopycnal coordinates. The stability of the modified schemes derived below is due in large part to this. For isopycnal coordinates the additional term proportional to δ_I is only zero when the mass fluxes are calculated using (54).

Linearising (55) one also finds that

$$
\frac{\partial \eta'}{\partial t} + u_1 \delta_x \overline{\eta'}^{x\nu_F} + v_1 \delta_y \overline{\eta'}^{y\mu_F} + H \left(\delta_x u' + \delta_y v' \right) = 0,
\tag{62}
$$

where H is the unperturbed depth.

4.3 Stability matrices

The properties of the numerical schemes are best analysed in terms of non-dimensional parameters. So it will be assumed that the perturbations are of a wave-like form

$$
(u', v', \eta') = (u_E, v_E, \eta_E) \exp\left(\frac{\mathrm{i}\kappa x}{\Delta x} + \frac{\mathrm{i}\lambda y}{\Delta y} - \mathrm{i}\omega f_0 t \right),
\tag{63}
$$

where ω is a non-dimensional frequency normalised using f_0, and κ and λ are non-dimensional horizontal wavenumbers for the x- and y-directions normalised using the grid spacings Δx and Δy respectively. As is usual in linearised stability calculations, physical

This article is protected by copyright. All rights reserved.

Accepted Article

quantities are given by the real parts of the above expressions and of those obtained below. Defining

$$c_p = \cos(p/2), \quad s_p = \sin(p/2), \quad p = \kappa, \lambda, \tag{64}$$

for any quantity ψ which varies with x, y and t in the same way as the quantities in (63) the x- and y-averaging operators give

$$\overline{\psi}^{x} = c_\kappa \psi, \quad \overline{\psi}^{y} = c_\lambda \psi, \tag{65}$$

and the differencing operators δ_x and δ_y give

$$\delta_x \psi = \frac{2\mathrm{i}}{\Delta x} s_\kappa \psi, \quad \delta_y \psi = \frac{2\mathrm{i}}{\Delta y} s_\lambda \psi. \tag{66}$$

It is convenient also to introduce the coefficients corresponding to the averaging operators,

$$\mu_E = \frac{1}{3}(1 + 2c_\kappa^2), \quad \nu_E = \frac{1}{3}(1 + 2c_\lambda^2). \tag{67}$$

and the associated modified coefficients which are given by

$$\begin{aligned} &\mu_F = \mu_E, \quad \nu_F = \nu_E \qquad \text{(modifiedscheme)}, \\ &\mu_F = \nu_F = 1 \qquad\quad \text{(originalscheme)}. \end{aligned} \tag{68}$$

One can define the other non-dimensional quantities in a number of different ways. A convenient approach is to define Froude numbers for the basic flows u_1 and v_1

$$F_u = \frac{u_1}{c}, \quad F_v = \frac{v_1}{c} \tag{69}$$

and to complete the set of non-dimensional parameters using

$$R_c = \frac{2c}{f_0 \Delta y}, \quad X = \frac{\Delta x}{\Delta y}. \tag{70}$$

R_c is twice the ratio of the Rossby radius (c/f_0) and the grid spacing Δy (the factor of 2 has been introduced to simplify expressions later) and X is the ratio of the grid-spacings. In models using latitude and longitude coordinates the latter ratio is small near the pole so the range $0 < X \leq 1$ is of interest. The grid-scale Rossby numbers R_u and R_v for the flows u_1 and v_1 can be constructed using the above parameters

$$R_u = \frac{2u_1}{f_0 \Delta x} = \frac{F_u R_c}{X}, \quad R_v = \frac{2v_1}{f_0 \Delta y} = F_v R_c. \tag{71}$$

We note that the factors of 2 in (71) result in values for R_u and R_v that are a factor of 2 larger than the values one would obtain using the classical definition of grid-scale Rossby numbers.

Substituting the above relations into the discrete linearised equations (61) and (62), after some algebra (doing normalizations using f_0, H, g and c), one obtains a matrix form of the stability problem

This article is protected by copyright. All rights reserved.

$$\begin{bmatrix} \omega - E_{11} & -\mathrm{i}c_\kappa c_\lambda - E_{12} & -\dfrac{R_c s_\kappa}{X} - \mathrm{i}E_{13} \\ \mathrm{i}c_\kappa c_\lambda - E_{21} & \omega - E_{22} & -R_c s_\lambda + \mathrm{i}E_{23} \\ -\dfrac{R_c s_\kappa}{X} & -R_c s_\lambda & \omega - E_{33} \end{bmatrix} \begin{bmatrix} u_E \\ v_E \\ \dfrac{c\eta_E}{H} \end{bmatrix} = 0. \tag{72}$$

where

$$\begin{aligned} E_{11} &= R_u s_\kappa c_\kappa \nu_F + R_v s_\lambda c_\lambda \mu_E, \\ E_{22} &= R_u s_\kappa c_\kappa \nu_E + R_v s_\lambda c_\lambda \mu_F, \\ E_{33} &= R_u s_\kappa c_\kappa \nu_F + R_v s_\lambda c_\lambda \mu_F, \\ E_{12} &= R_v X^{-1} s_\kappa c_\lambda (\mu_F - \mu_E), \\ E_{21} &= R_u X s_\lambda c_\kappa (\nu_F - \nu_E), \\ E_{13} &= \delta_I F_v c_\kappa c_\lambda^2 (\mu_F - \mu_E), \\ E_{23} &= \delta_I F_u c_\kappa^2 c_\lambda (\nu_F - \nu_E). \end{aligned} \tag{73}$$

In (72) the diagonal elements E_{11}, E_{22} and E_{33} represent advection of u', v' and η' respectively by the basic flow (u_1, v_1), $-c_\kappa c_\lambda$ in the same element as $\mathrm{i}E_{12}$ represents the Coriolis term $-f_0 v'$ in (102) and $c_\kappa c_\lambda$ in the same element as $\mathrm{i}E_{21}$ represents the Coriolis term $f_0 u'$ in (103). Note that the off-diagonal elements E_{12}, E_{21}, E_{13} and E_{23} are all equal to zero for the modified een scheme.

4.4 Stability of the modified een scheme

For the modified een scheme, because $E_{12} = E_{21} = E_{13} = E_{23} = 0$, the matrix equation (72) has the form

$$(\omega \mathbf{I} + \mathbf{H}) z = 0, \tag{74}$$

where $\mathbf{I}$ is the identity matrix and $\mathbf{H}$ is an Hermitian matrix, that is a matrix whose transpose is equal to its complex conjugate. All eigenvalues of Hermitian matrices are real-valued and hence the corresponding perturbations are neutrally stable. The eigenvectors of Hermitian matrices are also orthogonal (or can be chosen to be when two or more of the eigenvalues are identical). The gravity wave and Rossby wave solutions of (72) have different phase speeds and hence different eigenvalues so are automatically orthogonal. In conclusion the linear perturbations of the form (63) can be used to represent any initial conditions and the basic flow is neutrally stable to all linear perturbations.

4.5 Stability in isopycnal coordinates

Consider now the stability problem (72) for the original scheme using isopycnal coordinates ($\delta_I = 1$). It will be convenient to introduce

$$T_u \equiv R_u c_\kappa (1 - \nu_E), \quad T_v \equiv R_v c_\lambda (1 - \mu_E). \tag{75}$$

Using these definitions with (73) one sees that

This article is protected by copyright. All rights reserved.

Accepted Article

$$E_{11} = E_{33} - T_v s_\lambda, \quad E_{22} = E_{33} - T_u s_\kappa, \tag{76}$$

and (72) becomes

$$\begin{bmatrix} \varpi + T_v s_\lambda & -\mathrm{i}c_\kappa c_\lambda - T_v \dfrac{s_\kappa}{X} & -R_c \dfrac{s_\kappa}{X} - \mathrm{i}I_{13} \\ \mathrm{i}c_\kappa c_\lambda - T_u X s_\lambda & \varpi + T_u s_\kappa & -R_c s_\lambda + \mathrm{i}I_{23} \\ -R_c \dfrac{s_\kappa}{X} & -R_c s_\lambda & \varpi \end{bmatrix} \begin{bmatrix} u_E \\ v_E \\ \dfrac{c\eta_E}{H} \end{bmatrix} = 0. \tag{77}$$

in which

$$I_{13} \equiv c_\kappa c_\lambda T_v R_c^{-1}, \quad I_{23} \equiv c_\kappa c_\lambda T_u R_c^{-1} \tag{78}$$

and

$$\varpi = \omega - E_{33} = \omega - R_u s_\kappa c_\kappa - R_v s_\lambda c_\lambda \tag{79}$$

is the Doppler-shifted non-dimensional frequency of the perturbation.

By direct calculation of the determinant D_M of the matrix in (77), one finds that

$$D_M = \varpi^3 + P\varpi^2 - Q^2\varpi - PQ^2. \tag{80}$$

where

$$\begin{aligned} P &= T_u s_\kappa + T_v s_\lambda, \\ Q^2 &= c_\kappa^2 c_\lambda^2 + R_c^2 s_\kappa^2 X^{-2} + R_c^2 s_\lambda^2. \end{aligned} \tag{81}$$

Substituting $\varpi = -P$ into (80) one sees that it is a solution of $D_M = 0$. Hence it is easy to factorise (80),

$$D_M = (\varpi + P)(\varpi^2 - Q^2). \tag{82}$$

The solutions of $D_M = 0$ with $\varpi = \pm Q$ are the gravity waves and the solutions with $\varpi = -P$ are the Rossby waves and both sets of solutions are neutrally stable.

An interpretation of this result is presented in appendix 12.

4.6 Instabilities of the original schemes

There are of course general expressions for the solutions of the cubic equations derived from setting the determinant of the matrix in (72) to zero but the resulting expressions for the growth rates of the instabilities present in the original scheme are complicated and do not aid understanding. The expressions for instabilities aligned with the grid are much simpler than those for the general case so, following HKRB, these are considered first in this section. The solutions obtained numerically motivated the calculations for very small equivalent depths presented at the end of the section. The solutions are only presented for the een scheme but entirely analogous arguments and solutions hold for the AL scheme.

Instabilities aligned with the grid

We will consider instabilities that are aligned with the grid and without loss of generality take $\kappa = 0$ (rather than $\lambda = 0$). Both u_1 and v_1 will be allowed to be non-zero (which was not the case in HKRB). $\kappa = 0$ implies that $s_\kappa = E_{12} = 0$ and $c_\kappa = \mu_E = 1$. One then finds that $E_{13} = 0$ whether or not $\delta_I = 0$ and

This article is protected by copyright. All rights reserved.

Accepted Article

Accepted Article

$$E_{11} = E_{22} = E_{33} = R_v s_\lambda c_\lambda. \tag{83}$$

Consequently it is useful to introduce the Doppler-shifted non-dimensional frequency

$$\varpi = \omega - R_v s_\lambda c_\lambda. \tag{84}$$

Setting the determinant of the matrix in (72) for the original een scheme to zero, one of the solutions is $\varpi = 0$ and the other solutions have

$$\varpi^2 = a^2 + \mathrm{i}(1-\delta_I)J, \tag{85}$$

where

$$a^2 \equiv c_\lambda^2 + R_c^2 s_\lambda^2, \quad J \equiv F_u R_c s_\lambda c_\lambda (1-\nu_E). \tag{86}$$

Equations (85) and (86) are essentially the same as (6) in HKRB and are clearly a version of the dispersion relation for inertia-gravity waves. The final term on the rhs of (85) is purely imaginary and destabilises the inertia-gravity waves. When $\delta_I = 1$ this term is zero and the solutions for ϖ are all real. So the SWEs discretised using q in the Zu and Zv terms and isopycnal coordinate models should not suffer from symmetric instabilities of the kind discovered by [Hollingsworth ~al.(1983)Hollingsworth, Kallberg, Renner and Burridge]. This result is consistent with the comments made in [Arakawa(2000)] that were noted in the introduction and the results of the previous sub-section.

The dependence of the non-dimensional growth rate on the non-dimensional parameters for height coordinate models ($\delta_I = 0$) can be found by writing $\varpi \equiv \varpi_\mathrm{r} + \mathrm{i}\varpi_\mathrm{i}$ in (85) and eliminating ϖ_r:

$$2\varpi_\mathrm{i}^2 = -a^2 + \sqrt{a^4 + J^2}. \tag{87}$$

This solution to (72) has made no assumptions or approximations other than $\kappa = 0$.

The growth rate ϖ_i hence depends on the ratio J/a^2. When $J \approx a^2$ or $J >> a^2$, ϖ_i is relatively insenstive to a and to within 50%

$$\varpi_\mathrm{i}^2 \approx J/2, \quad a^2 \leq |J|. \tag{88}$$

This is the formula derived by HKRB for a slightly less general case. For the case with $a^2 >> |J|$, evaluating (87) using a Taylor series one finds that

$$\varpi_\mathrm{i} \approx \frac{|J|}{2a}, \quad a^2 >> |J|. \tag{89}$$

The equivalent depths and associated velocities c in the ocean vary greatly. Barotropic modes in water of 4 km depth have $c \approx 200\mathrm{ms}^{-1}$ whilst the first baroclinic mode has $c \approx 3\mathrm{ms}^{-1}$. As discussed in section 3, when the number of vertical levels is denoted by K, the highest vertical wavenumber mode in a model using the Charney-Phillips grid has $c \approx 3K^{-1}\mathrm{ms}^{-1}$ and in one using the Lorenz grid has $c \approx \frac{3}{2}\pi K^{-2}\mathrm{ms}^{-1}$. In a model with a 10 km grid at mid-latitudes $f\Delta x \approx 1\mathrm{ms}^{-1}$. Hence for the high wavenumber baroclinic modes $a^2 \approx c_\lambda^2$ and $J \approx XR_u$ and when X is of order 1 and R_u is larger than or of order 1 the growth rate, ϖ_i, is given by (88). For the barotropic modes $a \approx cs_\lambda/f_0$ and ϖ_i is given by (89).

For the baroclinic modes using (88), (86b), (64) and (67b) one sees that the most unstable perturbations have the largest values of

$$J = \frac{2}{3} F_u R_c \sin^3\frac{\lambda}{2}\cos\frac{\lambda}{2}. \tag{90}$$

This article is protected by copyright. All rights reserved.

Accepted Article

Differentiating J wrt λ one finds (in agreement with HKRB) that it is a maximum for the 3-gridpoint wave with

$$\lambda = \frac{2\pi}{3}, \quad J = \frac{\sqrt{3}F_u R_c}{2\sqrt{2}} \tag{91}$$

When $F_u R_c = XR_u >> 1$, as is often the case with modern grids, these modes can grow very rapidly. For example when $R_u = 10$, $J_{max} \approx 6$ and $\varpi_i \approx 3$. With $f_0 = 10^{-4}\mathrm{s}^{-1}$ the perturbation would increase by a factor of $\mathrm{e} \approx 2.7$ in $(f_0\varpi)^{-1}$ s which is about 3.3×10^3 s, i.e. just less than an hour.

For the barotropic modes

$$\varpi_i \approx \frac{|J|}{2a} = F_u c_\lambda (1-\nu_E) = \frac{2}{3}F_u \sin^2\frac{\lambda}{2}\cos\frac{\lambda}{2}. \tag{92}$$

Differentiating one finds that ϖ_i is a maximum when $\cos\lambda = 3^{-1/2}$. In the ocean F_u is typically less than or of order 0.01 and the maximum value of $\varpi_i = 4F_u/(9\sqrt{3})$.

Instabilities for very small Froude or Rossby numbers

Consider next the instabilities obtained in height coordinates when F_u and F_v are very small compared to R_u and R_v. For this case $E_{13} \approx E_{23} \approx 0$ and all the E_{ij} terms are proportional to R_u or R_v. As F_u and F_v tend to zero only the last element in the last row and the last column of the stability matrices remain non-zero. So the instabilities are determined by the determinant of the upper-left 2×2 sub-matrix.

In practice the growth rates of the instabilities are likely to be reduced by dissipative fluxes. Vertical diffusion of momentum is a parameterisation of an important physical process in ocean model which usually has large coefficients within the surface boundary layer and is a sufficiently fast process to need to be calculated implicitly. As the specification of the viscous coefficients varies considerably from one numerical model to another in the analysis below it is specified simply as being proportional to A_m, that is we set $A_m D_m u = -A_m u$ leaving the dependence on the vertical (and horizontal) wavenumbers of the disturbance for the reader to specify. These viscous dissipation terms only make contributions to the diagonal elements in the upper two rows of the stability matrix. The revised diagonal elements, E'_{11} and E'_{22} are given by

$$E'_{11} = E_{11} - \mathrm{i}A_m f_0^{-1}, \quad E'_{22} = E_{22} - \mathrm{i}A_m f_0^{-1}. \tag{93}$$

(a) (b)

Growth rates, ω_i, for the original een scheme using height coordinates for a flow aligned with the grid ($\nu_1 = 0$), $X = 1$ and $R_u = 10$ as functions of (a) κ with $\lambda = 2\pi/3$ and (b) λ with $\kappa = 0$.

Because the determinant in (72) reduces to just the upper-left 2×2 sub-matrix multiplied by $E_{33} - \omega$ the solutions consist of the Doppler-shifted "geostrophic" mode with $\omega = E_{33}$ and two other solutions which satisfy

$$\omega = \frac{E'_{11} + E'_{22}}{2} \pm S^{1/2}, \tag{94}$$

This article is protected by copyright. All rights reserved.

$$S \equiv \left(\frac{E'_{11}-E'_{22}}{2}\right)^2 - (\mathrm{i}c_\kappa c_\lambda + E_{12})(\mathrm{i}c_\kappa c_\lambda - E_{21}). \tag{95}$$

The first term in (94) is a Doppler-shifted frequency with a decay rate equal to $A_m f_0^{-1}$ which is what one might expect from the viscous dissipation. Evaluating S with $\kappa = 0$ one sees that, $s_\kappa = 0$, $\mu_E = 1$ and $E'_{11} = E'_{22}$, and hence that

$$S = -\mathrm{i}c_\lambda(\mathrm{i}c_\kappa c_\lambda - E_{21}) = c_\lambda^2 + \mathrm{i}\frac{2X}{3}R_u s_\lambda^3 c_\lambda. \tag{96}$$

When the imaginary part of S is non-zero one of the two solutions is unstable in the limit of small viscosity.

Evaluating $\partial S/\partial\kappa$ for any λ with $\kappa = 0$ one finds that

$$\frac{\partial S}{\partial \kappa} = 0. \tag{97}$$

This implies that $\partial\omega_\mathrm{i}/\partial\kappa = 0$ for any λ with $\kappa = 0$. This shows that the growth rates are stationary in the direction of κ when the perturbations are aligned with the grid. Taken with the numerical results it strongly suggests that the fastest growing perturbations are aligned with the grid for the limit of small Froude number.

An analysis of the instabilities when the Rossby number is very small can also be carried out. Denoting the eigenvalue solutions for $R_u = R_v = 0$ by ω_0, the gravity wave solutions have

$$\omega_0^2 = c_\kappa^2 c_\lambda^2 + R_c^2\left(s_\lambda^2 + \frac{s_\kappa^2}{X^2}\right), \tag{98}$$

and the Rossby waves have $\omega_0 = 0$. Linearising the determinant of the matrix in (72) about these solutions and writing $\omega = \omega_0 + \omega_1$, to first order in R_u and R_v one finds that the gravity waves have

$$\omega_{1\mathrm{i}} = \frac{c_\kappa c_\lambda}{2\omega_0}(E_{21} - E_{12}), \tag{99}$$

and the Rossby waves have $\omega_{1\mathrm{i}} = 0$.

4.7 Numerical evaluations of solutions of the stability matrices

Figure 4.6 presents numerical evaluations of the fastest growth rates obtained from (72) for a basic flow with $v_1 = 0$, using height coordinates ($\delta_I = 0$) with $R_u = 10$ and $X = 1$, for a number of values of F_u. The corresponding figure for the AL scheme is similar except that the non-dimensional maximum growth rate is approximately 1.2 rather than 1. Figure 4.6(a) plots the non-dimensional growth rates ω_i as a function of κ with $\lambda = 2\pi/3$ and figure 4.6(b) plots ω_i as a function of λ with $\kappa = 0$. From Figure 4.6(a) it is apparent that when $F_u >> 1$ the fastest growing disturbances have $\kappa << 1$. Figure 4.6(b) shows that the maximum non-dimensional growth rate when $F_u = R_u = 10$ is close to 1. These disturbances increase in magnitude by a factor of $\mathrm{e} \approx 2.7$ in f_0^{-1} s. At mid-latitudes $f_0^{-1} \approx 10^4$ s which is just less than 3 hours. From figure 4.6 it is also clear that the growth rate at the chosen value of R_u is strongly dependent on

This article is protected by copyright. All rights reserved.

Accepted Article

Accepted Article

the Froude number (F_u) being weak when $F_u < 0.1$ and strong when $F_u > 5$. High values of the Froude number are obtained for the highest vertical modes, particularly on the Lorenz grid.

Figure 3: Growth rates, ω_i, for the original een scheme using height coordinates for a flow aligned with the grid ($v_1 = 0$), $X = 1$, $R_u = 10$ and $F_u = 10$ as functions of λ with $\kappa = 0$. Blue solid line: eq (72). Red dash-dot line line: eq (88). Green dashed line: eq (89).

Figure 3 provides a comparison of the solutions of (88) and (89) with those of (72) calculated using $F_u = R_u = 10$ and $X = 1$. The green lines are solutions of (89) with $|J| < a^2$ and the blue line is the solution of (72). Clearly the agreement is good. The red line in figure 3 is the solution of (89). This solution depends only on R_u and is expected to hold only when F_u is very large. Comparing figures 4.6(b) and 3 one sees that the approximation requires F_u to be very large to be accurate.

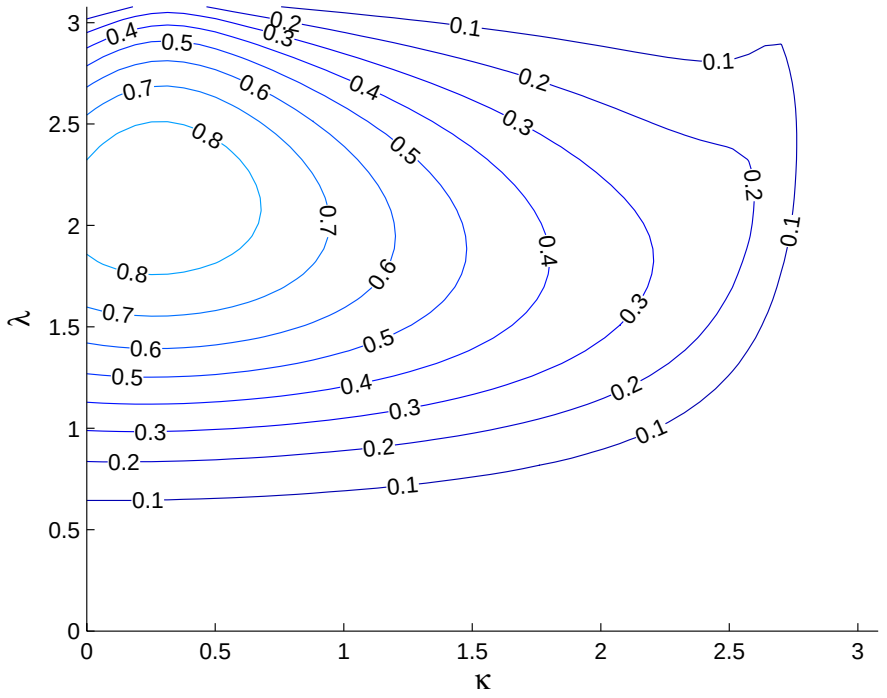

(a) $R_u = 10$, $F_u = 10$ (b) $R_u = 10$, $F_u = 40$

(c) $R_u = 40$, $F_u = 10$ (d) $R_u = 40$, $F_u = 40$

Figure 4: The fastest growing instabilities (maximum $|\omega_i|$) for varying λ and κ for the original een scheme in height coordinates for the case with $v_1 = 0$ and four combinations of R_u and F_u.

This article is protected by copyright. All rights reserved.

Accepted Article

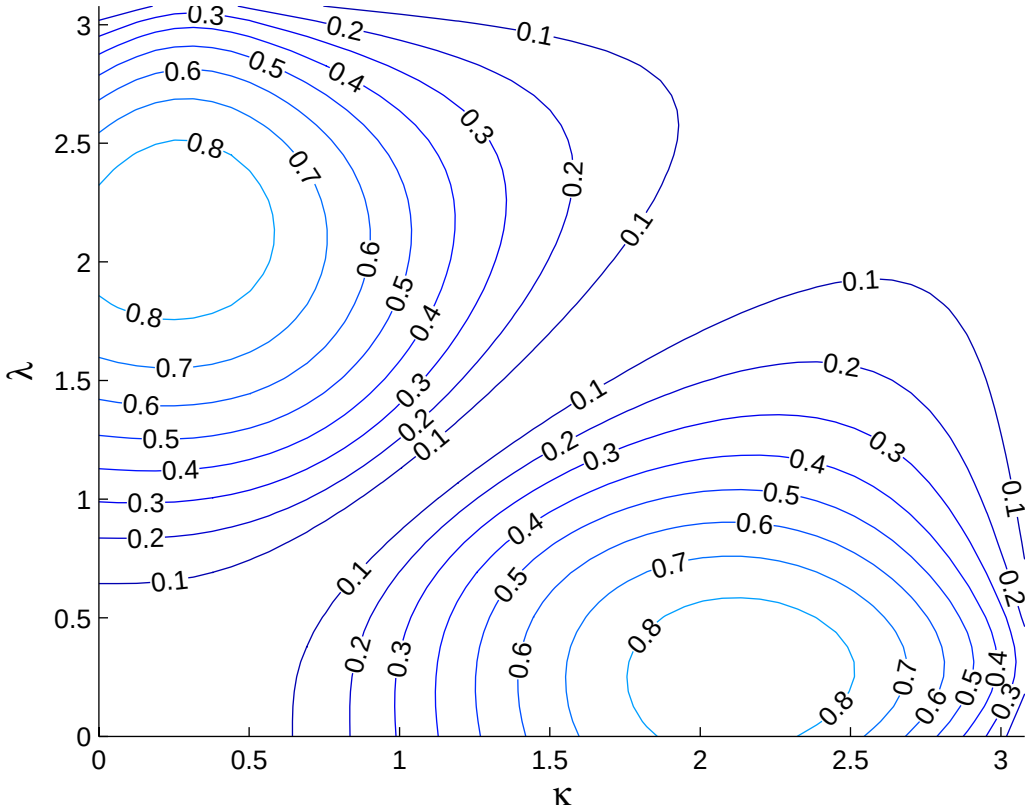

Figure 4 illustrates the growth rates of the unstable solutions of (72) for the original een scheme using height coordinates as a function of κ and λ for four combinations of R_u and F_u when $X = 1$. The fastest growing solutions have growth rates similar to the fastest growing solutions with $\kappa = 0$ and their wavenumber is quite closely aligned with the λ-axis particularly when F_u is large.

(a) (b)

Figure 5: The fastest growing instabilities for all λ and κ for the original een scheme in height coordinates for the case with $v_1 = 0$ as a function of F_u (on the abscissa) and R_u; (a) the maximum growth rates, ω_1 and (b) their wavenumber (κ, λ); the arrows show their direction and the contours their magnitude.

This article is protected by copyright. All rights reserved.

Accepted Article

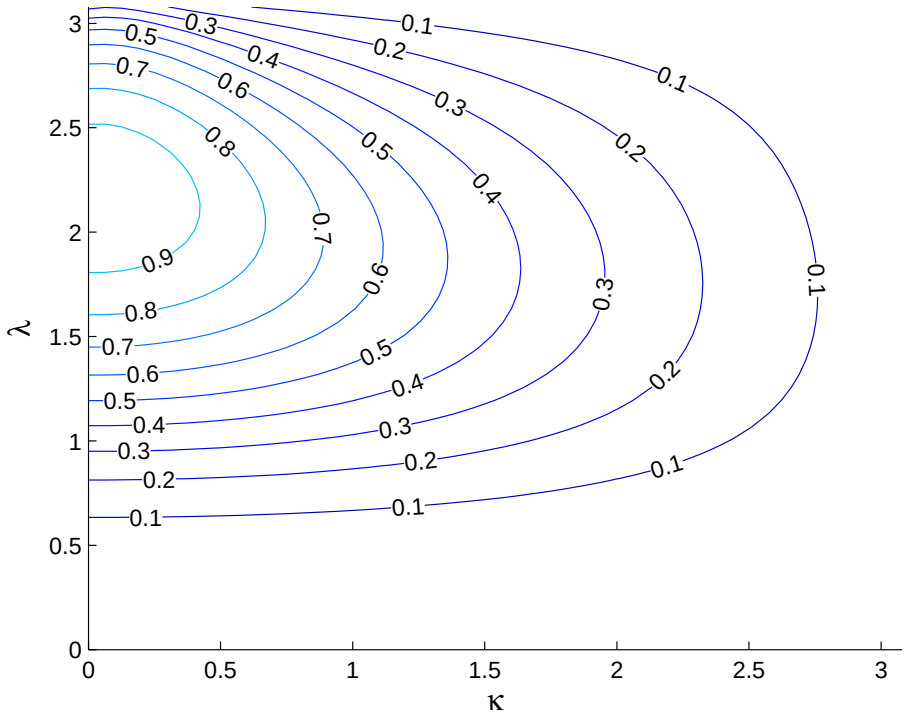

Figure 5(a) shows the maximum values of ω_i obtained for all κ and λ as a function of F_u, on the abscissa, and R_u when $X = 1$. The largest growth rates are obtained when both F_u and R_u are large, values of ω_i as large as 2.2 being obtained when $R_u = F_u = 50$. These perturbations take less than 90 minutes to double in amplitude at mid-latitudes. The corresponding plot (not shown) of maximum growth rates for perturbations restricted to those with $\kappa = 0$ is barely distinguishable by eye from figure 5(a). Figure 5(b) shows the direction and magnitude of the wavenumber (κ, λ) of the fastest growing perturbations. These perturbations have $\kappa \approx 0$ and the wavenumber of maximum growth rate $\lambda \approx 2.1$ is consistent with the findings of HKRB and (91). When $X = 0.1$ the fastest growing disturbances also have $\kappa \approx 0$ but the maximum growth rates are somewhat smaller (their maximum being of order 0.9 for the range of F_u and R_u plotted in figure 5(a)).

Figure 6 is the same as figure 5 except that it shows the maximum growth rates for the AL scheme rather than the een scheme. The plot of maximum growth rate for symmetric disturbances only corresponding to figure 6a is again not shown because they are barely distinguishable. (a) (b)

Figure 6: The same as Figure 5 except that the results are for the AL scheme rather than the een scheme.

This article is protected by copyright. All rights reserved.

Accepted Article

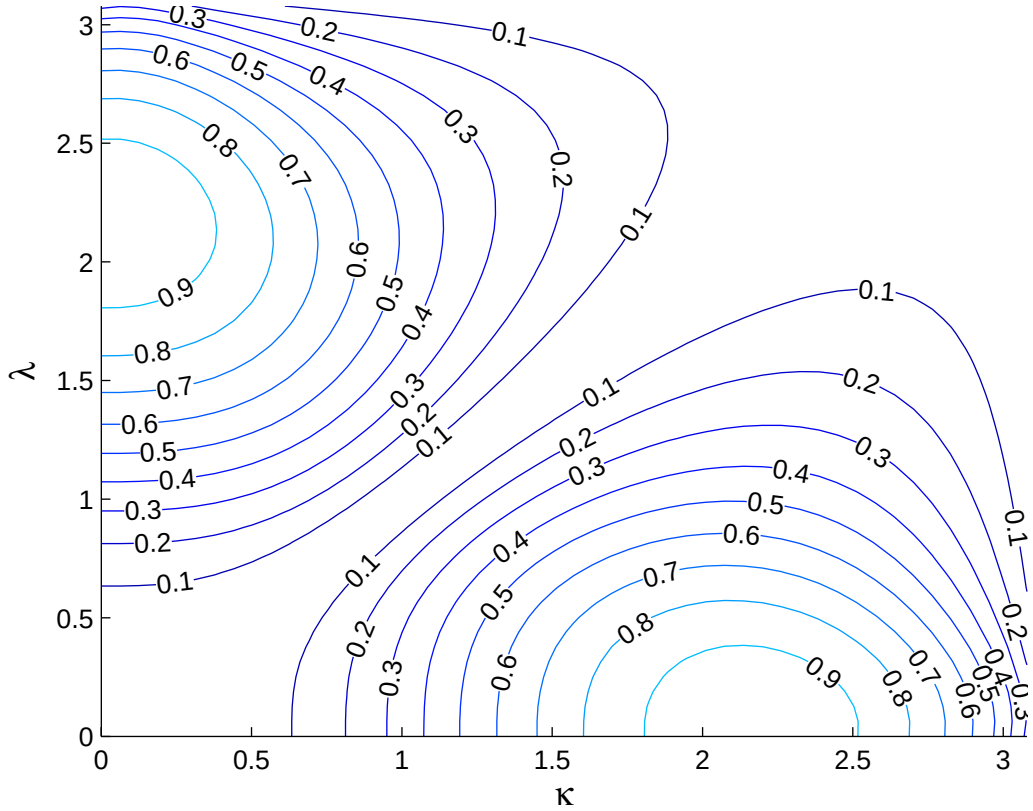

Figure 7 is the same as figure 4 except that it was obtained using $v_1 = u_1$ instead of $v_1 = 0$. It is symmetric about the line $\kappa = \lambda$ as one would expect from the symmetries of the problem. More interesting is that it shows that the most unstable perturbations are aligned with the grid rather than the background flow, the alignment again being particularly strong when $F_u >> 1$. The figures for this case corresponding to figure 5 for the een scheme and figure 6 for the AL scheme are not shown because they are barely distinguishable from those already presented except that when $u_1 = v_1$ there are two maxima, the second being obtained from the single maximum present for $v_1 = 0$ by reflection in $\kappa = \lambda$. (a) $R_u = 10$, $F_u = 10$ (b) $R_u = 10$, $F_u = 40$

This article is protected by copyright. All rights reserved.

Accepted Article

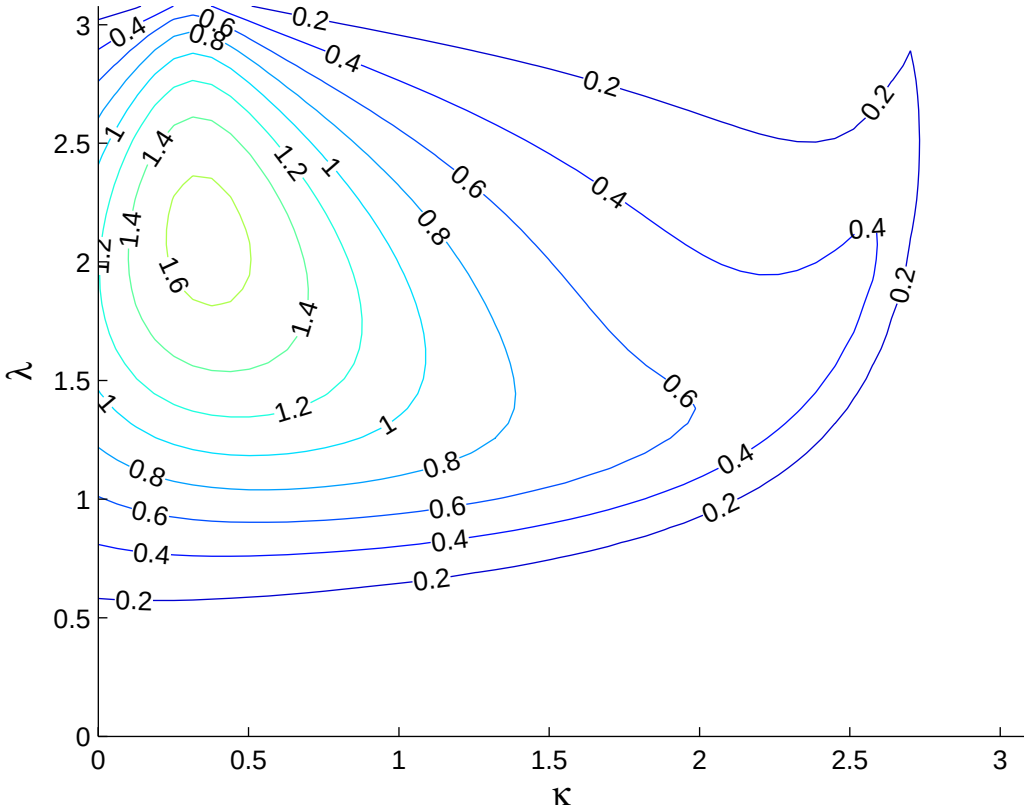

(c) $R_u = 40$, $F_u = 10$ (d) $R_u = 40$, $F_u = 40$

Figure 7: The fastest growing instabilities (maximum $|\omega_i|$) for varying λ and κ for the original een scheme in height coordinates for the case with $v_1 = u_1$ and selected values of R_u and F_u.

Numerical solutions of (72) strongly suggest that all linear disturbances to a flow in any direction are neutrally stable for the original schemes in isopycnal coordinates. This result motivated the analysis presented in section 4.5.

5 Numerical analyses of the SWE

To investigate the instability using the fully nonlinear shallow water equations, we implemented the een scheme (as described in sub-section 4.1) on a [0,1]×[0,1] doubly periodic plane with an explicit fourth order four stages Runge-Kutta time-integration scheme. The model was validated using initial conditions given by $u = \sin(2\pi y)$, $v = 0$ and h chosen to balance with u. Second order accuracy in space and conservation of total energy and total potential enstrophy within time truncation errors was achieved on all 4 configurations tested: original and modified schemes, with height and isopycnal coordinates.

This article is protected by copyright. All rights reserved.

Accepted Article

One of the main outcomes of this study is that the developer of a new numerical scheme should be able to test whether it will suffer from Hollingsworth type instabilities in a shallow water model context, rather than having to wait for a fully 3D version of the scheme to be developed. The key point is to use uniformly small equivalent depths which slow down the gravity waves and highlight nonlinear effects. A similar approach was discussed by [Gassmann(2011)] in an investigation of the divergence of computational modes on triangular grids. To help researchers track the instability at the shallow water development stage, we propose two test cases.

5.1 Instabilities on a constant zonal flow

In this first test case we used a constant initial zonal flow, a flat bottom ($z_b = 0$ in (31)) and an additional forcing term equal to $f_0 u_1$ on the rhs of (30b) to produce a balanced steady state solution (parameters $u_1 = 50\Delta x$, $H = 2.5\Delta y^2$, $f_0 = 10$, $g = 10$, $\Delta x = \Delta y = 1/64$ and timestep $\Delta t = 1/1024$ which give $R_u = 10$ and $F_u = 10$). To trigger the instability, we added a small perturbation to η at the central point of the domain (we used $+H/1000$). The modified scheme in height coordinates and both schemes in isopycnal coordinates did not reveal any instabilities in the tests performed. However, the height coordinate model with the original een scheme suffers from instabilities with a dominant non-dimensional wavenumber λ, of approximately $2\pi/3$ which grow in amplitude by a factor larger than 10^3 for every nondimensional time unit (see Figure 8). Taking the difference from the initial state, $E(t)$, to grow exponentially with time at a rate given by $\omega_1 f_0$ and fitting a straight line through the right panel of figure 8 we obtain an approximate value for ω_1 of 0.8, in very good agreement with figure 3b.

Figure 8: Shallow water model run with height coordinates, the original een scheme, an initially constant water depth, a constant zonal initial velocity, zonally symmetric forcing to keep the system in a steady state, and a small perturbation in the center of the domain. On the left: Spectrum of a y-slice of η, where the wavenumbers were normalized to $(0,\pi)$. On the right: evolution of $E_\eta(t)$, the maximum difference from the initial state of the layer depth η.

This article is protected by copyright. All rights reserved.

Accepted Article

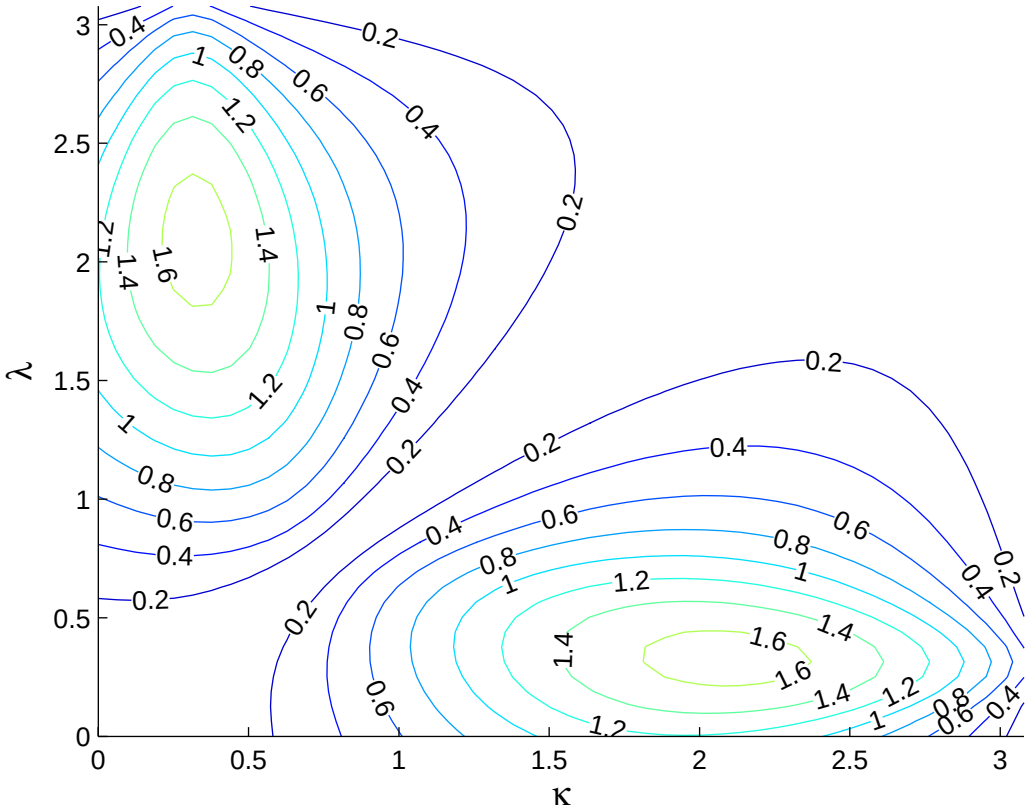

5.2 Instabilities on a sinusoidaly varying zonal flow

Figure 9: Shallow water model run with height coordinates, the original een scheme, an initially constant water depth and sinusoidal zonal velocity with a bottom topography which keeps the zonal flow in balance. On the left: Spectrum of a y-slice of η, where the wavenumbers were normalized to $(0,\pi)$. On the right: evolution of $E_\eta(t)$, the maximum difference from the initial state of the layer depth η.

This article is protected by copyright. All rights reserved.

Accepted Article

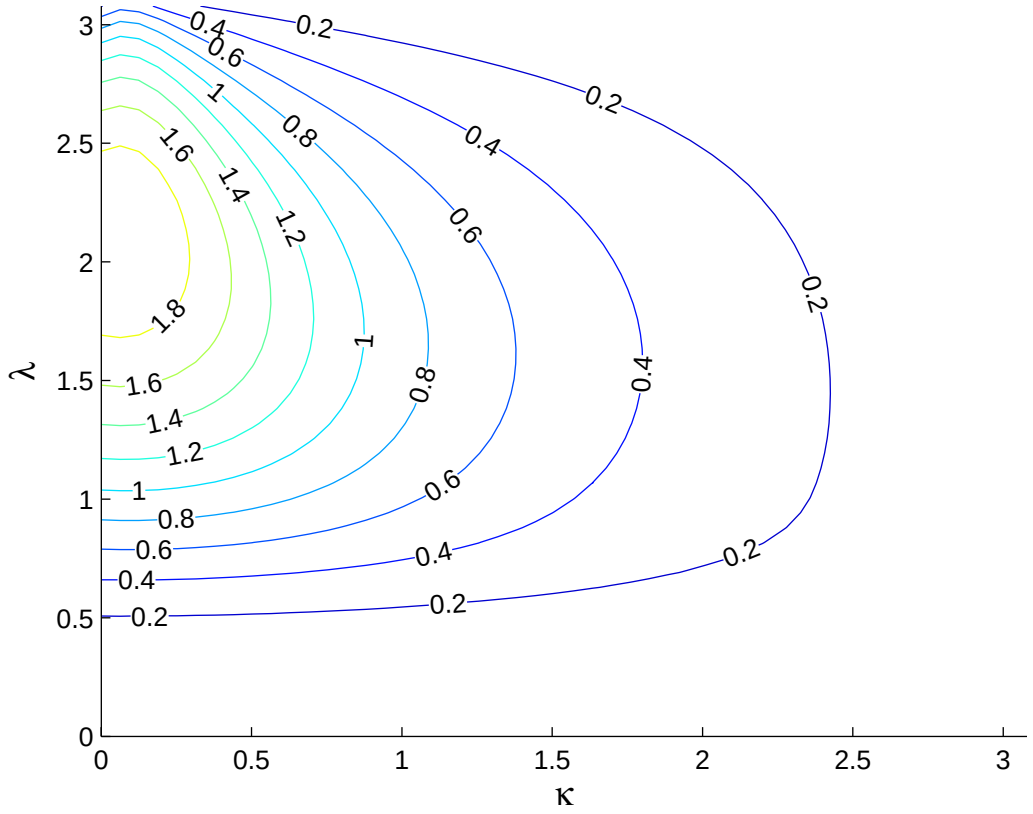

In this second test case we set the zonal velocity $u(x,y) = u_1 \sin(2\pi y)$, and $h(x,y) = h_0$, where both u_1 and h_0 are constants. In order to create a steady state solution, the bottom topography (bathymetry) is set to $z_b(x,y) = \frac{u_1 f_0}{2\pi g}\cos(2\pi y)$. Since the prognostic variables are functions only of y, the solution is independent of x, and the shallow water equations reduce to a 1D problem. The only initial source of error is due to the non cancellation of the nonlinear terms in the evolution equation for v. For appropriate choices of the parameters, the instability afflicts the height coordinate model with the original een scheme, as expected. We show in figure 9 an example (parameters $u_1 = 10$, $H = 0.1$, $f_0 = 1/\Delta x$, $g = 10$, $\Delta x = \Delta y = 1/64$ and $dt = 1/1024$ which give $R_u = 20$ and $F_u = 10$) of the spectrum a few time steps before the model blows up, and also the evolution with time of the maximum error in the layer thickness (η) (i.e. the maximum difference from its original value). The initial condition is dominated by a low wavenumber pattern (wave number 2), but as time evolves, errors in higher wavenumbers appear and the instability is triggered. Once triggered, the growth rates are very large. The estimated non-dimensional growth rate for the parameters used in figure 9 is $\omega_i \approx 2.0$. This test case has non zero relative vorticity and growth rates that are somewhat larger than those obtained using the formulae for a constant flow on an f-plane. Figure 10 provides a snapshot of the model fields at a time when the instability is emerging in the h and v fields.

Figure 10: The fields from the same integration as figure 9 at a time $t = 0.35$ when the

This article is protected by copyright. All rights reserved.

Accepted Article

instability is emerging. Blue lines indicate the field values at $t = 0.35$, and the red (green) line indicates the maximum (minimum) value attained earlier in the integration.

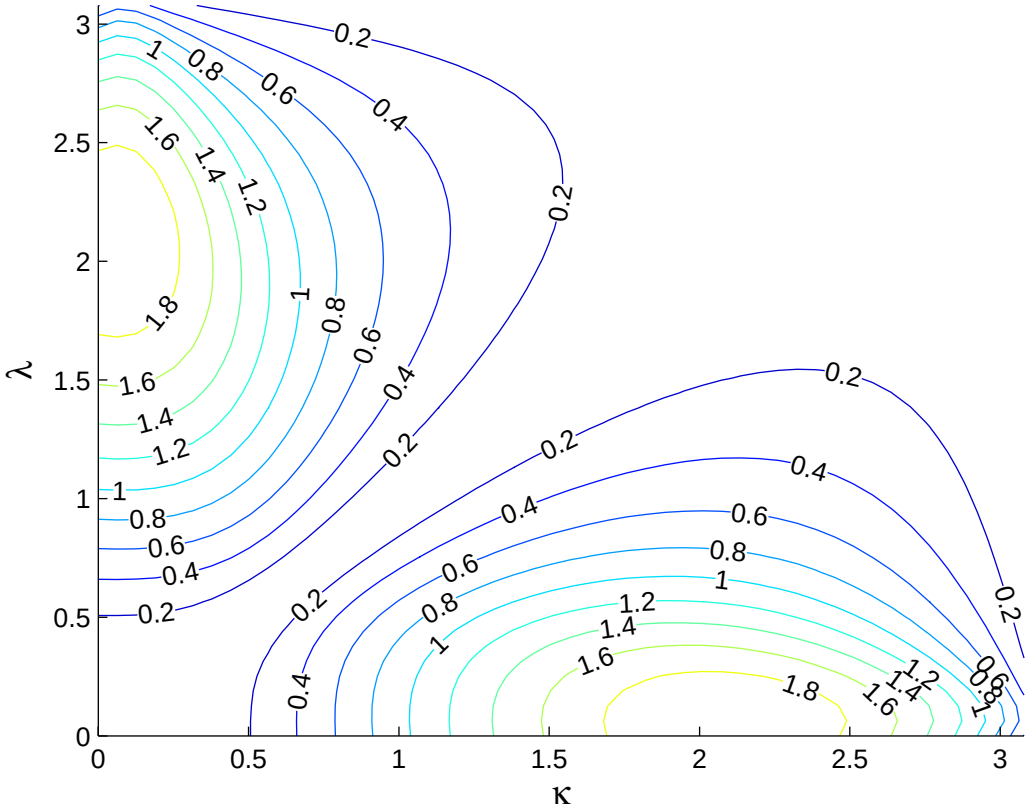

6 Concluding summary and discussion

The factors that determine the linear stability of constant flows on an f-plane to grid-scale disturbances have been clarified for a number of discretisations of the vector invariant momentum equations which use regular rectangular grids in the horizontal. The 3D stability problems obtained in height coordinates and isopycnal coordinates have been confirmed to be soluble as a linear combination of products of a vertical mode and a solution of linearised shallow water equations (SWEs) with the depth H of the water determined by the eigenvalue of the vertical mode. Two dimensional SWEs which can be used to explore the stability of new 3D dynamical cores written in height or isopycnal coordinates have also been identified.

The depth H of the SWE associated with the modes of highest vertical wavenumber obtained using the Lorenz grid decreases more rapidly as the number of depth levels increases than is the case for solutions obtained using the Charney-Phillips grid, for reasons related to the occurrence of the computational mode on the Lorenz grid.

The 3×3 matrices which determine the linear stability of the een (energy and enstrophy conserving) scheme (and the AL scheme) both in their original and modified forms and in height and isopycnal coordinates have been constructed. It has been shown that these stability problems for all the modified schemes can be written as eigenvalue problems for Hermitian matrices and

This article is protected by copyright. All rights reserved.

Accepted Article

hence that all the modified schemes are neutrally stable. The instabilities obtained for the original schemes in height coordinates grow most rapidly when the Froude number and the grid-scale Rossby numbers are large and the instability is nearly aligned with the grid.

Simple expressions for the growth rates have been obtained for instabilities aligned with the grid and for instabilities when the Froude number or the Rossby number is very small. Our numerical investigations of the original schemes for isopycnal coordinates found that they do not suffer from Hollingsworth instabilities, in agreement with [Arakawa(2000)]. The determinant of the stability matrix for this case has been shown to reduce to a simple factorisable form which has real solutions and an explanation of this result has been proposed in terms of solutions of the linearised SWEs with uniform potential vorticity (appendix 12).

As shown by HKRB (see the discussion following (85) and (86)) the instabilities are inertia-gravity waves that have been destabilised by the discretisation of the generalised Coriolis terms. Consequently, and consistent with the discussion in appendix B of [Gassmann(2013)], one would not expect quasi-geostrophic models (which do not represent inertia-gravity waves) to suffer from them. [Gassmann(2013)] notes that the instabilities occur preferentially in regions of high vertical shear where the stratification is relatively weak and the phase speeds of the internal modes are consequently relatively slow. The Froude number will be highest in these regions so, provided the Rossby number is high enough, the instabilities will grow more rapidly in these regions.

Our results show that basic states that have no horizontal temperature gradients (and associated vertical shear in the horizontal velocity) can suffer from the Hollingsworth instability when discretised using the een or AL schemes and height coordinates. High vertical shear and high horizontal velocity tend to occur near to each other, so in practice it will be difficult to distinguish whether an instability seen in a model is associated with one rather than the other, especially when other factors (stratification, vertical grid spacing) are also implicated. The instabilities can be obtained in height coordinates if a C-P vertical grid is used with a large number of vertical levels but will usually grow faster on a Lorenz grid (with the same number of vertical levels) because the equivalent depth of the most rapidly varying modes is then much smaller and the Froude number much larger. These instabilities do not occur for these simple states discretised using isopycnal coordinates but this does not rule out the possibility that other instabilities owing their existence to discretisation issues rather than physical causes may occur on more complex flows, for example on a β-plane or the sphere or, as found by [Arakawa and Moorthi(1988)], on flows with vertical shear.

The origin of the instabilities in height coordinates might be attributed to a a loss of some form of momentum conservation, as suggested by HKRB, or to the loss of the invariance of the momentum equations to uniform motion of the frame of reference. As suggested (but not proved) by HKRB and AL, by smoothing the kinetic energy in the Bernoulli potential using a stencil similar to that used in the generalised Coriolis terms one can obtain a modified scheme which is stable to all disturbances. The instabilities for the original schemes grow extremely rapidly when the Froude number and Rossby number are very large but sufficient cancellation of terms may be possible using this approach on other (e.g. hexagonal) grids as suggested by [Gassmann(2013)].

It is hoped that the above results will help developers of new dynamical schemes (e.g. on triangular, hexagonal and other meshes) to test their schemes using appropriately configured SWEs and to devise modified schemes which do not suffer from Hollingsworth instabilities.

We gratefully acknowledge inputs from Nicolas Ducousso, Gurvan Madec, Julien le Sommer, David Storkey, Andy White and Nigel Wood. Bell was supported by the Joint UK

This article is protected by copyright. All rights reserved.

Accepted Article

DECC/Defra Met Office Hadley Centre Climate Programme (GA01101), Peixoto acknowledges the Sao Paulo Research Foundation (FAPESP), under the grant number 2014/10750-0 and Thuburn was supported by the Natural Environment Research Council under grant number NE/K006762/1.

Appendix

7 Notation

Tables 1 - 3 summarise the notation used in the main body of the paper. The third column of the tables refers to the equations where symbols are first introduced.

Table 1: Table of Greek symbols for primary variables

Greek - Lower case		
δ_ι	a difference operator	(50)
δ_I	Kronecker delta function	(59)
ζ	vertical component of the relative vorticity	(2)
η	height of the free surface	(9)
ι	the grid index in any direction	(50)
κ, λ	wavenumbers of perturbation in x - and y - directions	(63)
μ	coefficients from averaging in x	(52)
ν	coefficients from averaging in y	(52)
ξ	a coordinate in any direction	(50)
ϖ	Doppler shifted non-dimensional frequency	(79), (84)

This article is protected by copyright. All rights reserved.

Accepted Article

ρ	density	(4)
σ	inverse of stratification in isopycnal model	(19)
ψ	any function of ξ	(50)
ω	non-dimensional frequency of perturbation	(63)
Greek - Upper case		
Δ	the difference between neighbouring grid points	(50)
Λ	a non-dimensional parameter for vertical modes	(41)
Φ	the Bernoulli function	(3)

Table 2: Table of Roman symbols for primary variables

Roman - Lower case		
a	a parameter	(86)
b	buoyancy	(19)
c	speed $c^2 = gH$	
c_κ, c_λ	cosines of wavenumbers	(64)
f	the Coriolis parameter	(2)
g	gravity	(4)
h	function of z related to w or z	(14), (109)

This article is protected by copyright. All rights reserved.

Accepted Article

m, n	constants related to equivalent depths	(42), (43)
p	pressure	(3)
q	potential vorticity	(22)
$s_\kappa,\ s_\lambda$	sines of wavenumbers	(64)
t	time	(5)
u, v, w	velocity components	(5)
x, y	horizontal coordinates	(2)
z	height coordinate	(4)
Roman - Upper case		
A_m	coefficient of viscosity	(5)
D_M	determinant	(80)
D	total derivative (as in D/Dt)	(6)
D_m	diffusive operator	(5)
E_{ij}	matrix element for een scheme	(73)
F_u, F_v	Froude numbers	(69)
H	the total depth (or equivalent depth)	(12)
$\mathbf{H}$	an Hermitian matrix	(74)
$\mathbf{I}$	the identity matrix	(74)
J	a non-dimensional quantity	(86)
K_e	horizontal kinetic energy	(1)
K	the number of vertical levels	(37)
M	Montgomery	(20)

This article is protected by copyright. All rights reserved.

Accepted Article

	potential	
$N-1$	the number of zeros in the vertical	(45)
P, Q	coefficients	(81)
R_c	twice the ratio of the Rossby radius and grid spacing	(70)
R_u , R_v	Rossby numbers	(71)
S	a non-dimensional quantity	(96)
T_u , T_v	modified Rossby numbers	(75)
X	grid aspect ratio	(70)
W	a constant in normal mode soln	(44)
Z	vertical component of the total vorticity	(2)

Table 3: Table of subscripts and superscripts

Subscripts		
b	the (height of the) bottom	(31)
e	equivalent (as in H_e)	(12)
i	imaginary part	(87)
i, j	x - and y coordinate indices	(50)
k	the vertical index	(34)
x, y	horizontal	(50), (51)

This article is protected by copyright. All rights reserved.

	coordinates	
E	een scheme	(52)
F	modified een scheme	(53)
I	isopycnal	(59)
M	matrix	(80)
00	constant density	(3)
0	the stably stratified component of the basic state	(100)
1	the constant velocity component of the basic state	(101)
Superscripts		
μ	averaging in x	(52)
ν	averaging in y	(52)

Accepted Article

This article is protected by copyright. All rights reserved.

	a perturbation	(9), (102)

Accepted Article

This article is protected by copyright. All rights reserved.

Accepted Article

*	transports through faces of cells	(22), (33)
$\hat{\phi}$	a function of the vertical coordinate	(9)
$\tilde{\phi}$	a function of x, y and t	(9)
$\bar{\phi}$	an average of ϕ	

8 Separation of variables in height model

8.1 Basic state and perturbed equations

Assuming the basic state of a stably stratified density field $\rho_0(z)$ as described in section 2.1, we have that

$$\frac{\mathrm{d}p_0}{\mathrm{d}z} = -\rho_0 g, \tag{100}$$

and

$$p_1 = f\rho_{00}(v_1 x - u_1 y). \tag{101}$$

Denoting the perturbations by primed quantities and neglecting products of perturbations the horizontal momentum equations for the perturbations are given by

$$\frac{\partial u'}{\partial t} - f_0 v' - \zeta' v_1 = -\frac{\partial \Phi'}{\partial x} + A_m D_m u', \tag{102}$$

$$\frac{\partial v'}{\partial t} + f_0 u' + \zeta' u_1 = -\frac{\partial \Phi'}{\partial y} + A_m D_m v'. \tag{103}$$

where

$$\zeta' = \frac{\partial v'}{\partial x} - \frac{\partial u'}{\partial y}, \quad \Phi' = \frac{p'}{\rho_{00}} + (u_1 u' + v_1 v'). \tag{104}$$

Hydrostatic balance for the perturbations is

$$\frac{\partial p'}{\partial z} = -\rho' g, \tag{105}$$

the incompressibility condition is

$$\frac{\partial u'}{\partial x} + \frac{\partial v'}{\partial y} + \frac{\partial w'}{\partial z} = 0, \tag{106}$$

and the density perturbations satisfy

This article is protected by copyright. All rights reserved.

$$\frac{\partial \rho'}{\partial t} + u_1 \frac{\partial \rho'}{\partial x} + v_1 \frac{\partial \rho'}{\partial y} + w' \frac{\mathrm{d}\rho_e}{\mathrm{d}z} = 0, \tag{107}$$

because the heating by dissipation is zero in (107) when the basic state has no shear. Finally the boundary conditions are

$$w' = 0, \quad z = 0, -H_0. \tag{108}$$

In summary the above set has five unknowns u', v', w', ρ' and p' that are constrained by five equations and the boundary conditions (108).

8.2 Separable solutions

Comparing the five equations just summarised with those in section 6.11 of [Gill(1982)] one sees that they enjoy separable solutions of the same form. Departing slightly from the order of Gill's derivation we assume that the variations in u', v' and p' are given by (9). Then $g\rho_{00}\Phi' = \hat{p}(z)\tilde{\Phi}(x,y,t)$ where $\tilde{\Phi}$ is given by (11) and the horizontal momentum equations reduce to (10).

Following Gill we let

$$\rho' = \hat{\rho}(z)\tilde{\eta}, \quad w' = \hat{h}(z)\tilde{w}(x,y,t). \tag{109}$$

Substituting (9c) and (109a) into (105) we obtain (13). Substituting (109) into (107) and introducing the separation constant H_e we obtain (14) and

$$H_e \tilde{w} = \frac{\partial \tilde{\eta}}{\partial t} + u_1 \frac{\partial \tilde{\eta}}{\partial y} + v_1 \frac{\partial \tilde{\eta}}{\partial y}, \tag{110}$$

Substituting (9) and (109b) into (106) we can choose to set (15) and obtain

$$\left(\frac{\partial \tilde{u}}{\partial x} + \frac{\partial \tilde{v}}{\partial y} \right) + \tilde{w} = 0. \tag{111}$$

Eliminating $\tilde{w}$ from (111) using (110) we obtain (12).

Hence the solutions dependent on x, y and t are governed by the shallow water equations (10) and (12). The vertical structure functions $\hat{h}(z)$, $\hat{\rho}(z)$ and $\hat{p}(z)$ are determined by (13) (14) and (15) and the boundary conditions (16) obtained from (108) and (109).

9 Separation of variables in isopycnal model

9.1 Basic state and perturbed equations

The assumed basic state is the same as that in the previous section. Here we just adjust the notation. So, the stably stratified state is expressed as a profile $z_0(b)$ that is in hydrostatic balance

$$\frac{\mathrm{d}M_0}{\mathrm{d}b} = -z_0. \tag{112}$$

The horizontal velocity field (u_1, v_1) is again in geostrophic balance with a pressure field p_1 so,

$$M = M_0(b) + M_1, \quad M_1 = f(v_1 x - u_1 y). \tag{113}$$

This article is protected by copyright. All rights reserved.

Accepted Article

Accepted Article

The relative vorticity is again zero and the total vorticity, $Z_0 = f_0$, is independent of position.

The horizontal momentum equations for the perturbations are given by

$$\frac{\partial u'}{\partial t} - f_0 v' - \zeta' v_1 - \frac{f_0 v_1}{\sigma_0}\left(\sigma'^{(v)} - \sigma'^{(q)}\right) = -\frac{\partial \Phi'}{\partial x}, \tag{114}$$

$$\frac{\partial v'}{\partial t} + f_0 u' + \zeta' u_1 + \frac{f_0 u_1}{\sigma_0}\left(\sigma'^{(u)} - \sigma'^{(q)}\right) = -\frac{\partial \Phi'}{\partial y}. \tag{115}$$

where ζ' is given by (104a) and

$$\Phi' = M' + (u_1 u' + v_1 v'). \tag{116}$$

From (23), hydrostatic balance for the perturbations is given by

$$\frac{\partial M'}{\partial b} = -z'. \tag{117}$$

Continuity of mass, (24), gives

$$\frac{\partial \sigma'}{\partial t} + u_1 \frac{\partial \sigma'}{\partial x} + v_1 \frac{\partial \sigma'}{\partial y} = -\sigma_0 \left(\frac{\partial u'}{\partial x} + \frac{\partial v'}{\partial y} \right), \tag{118}$$

and the boundary conditions, (25), become

$$\frac{\partial z'}{\partial t} + u_1 \frac{\partial z'}{\partial x} + v_1 \frac{\partial z'}{\partial y} = 0, \quad b = b(0), b(-H). \tag{119}$$

In summary the above set has four unknowns u', v', M' and z' that are constrained by four equations and the above boundary conditions.

9.2 Separable solutions

Let

$$\begin{aligned} &u' = \hat{M}(b)\tilde{u}(x,y,t), \quad v' = \hat{M}(b)\tilde{v}(x,y,t), \\ &M' = \hat{M}(b) g \tilde{\eta}(x,y,t). \end{aligned} \tag{120}$$

Then

$$\Phi' = \hat{M}(b)\tilde{\Phi}(x,y,t), \quad \tilde{\Phi}(x,y,t) = g\tilde{\eta} + u_1\tilde{u} + v_1\tilde{v}, \tag{121}$$

and the terms in (114) and (115) other than those involving σ' reduce to (26). These additional terms will be considered shortly.

Letting

$$z' = \hat{h}(b)\tilde{\eta}, \tag{122}$$

and substituting (120c) and (122) into (117) gives (27). Substituting (120) and (122) also into (118) and introducing the separation constant H_e one obtains (12) and (28).

The vertical structure of the additional terms in the horizontal momentum equations can now be considered. Using (19) and (28) one sees that their vertical structure is given by

$$\frac{\sigma'}{\sigma_0} = \frac{\tilde{\eta}}{\sigma_0}\frac{\mathrm{d}\hat{h}}{\mathrm{d}b} = \frac{\tilde{\eta}\hat{M}}{H_e} \tag{123}$$

Hence these additional terms have the same vertical structure as the other terms in the momentum equations and (114) and (115) reduce to (26).

Finally the boundary conditions obtained from (119) and (122) reduce to (29).

This article is protected by copyright. All rights reserved.

Accepted Article

10 The een scheme horizontal discretisation

The een scheme calculates qv^* at the central u point in Figure 11, located at $(i, j+1/2)$, as the sum of products of quantities calculated at the surrounding v points (A, B, C and D in the figure)

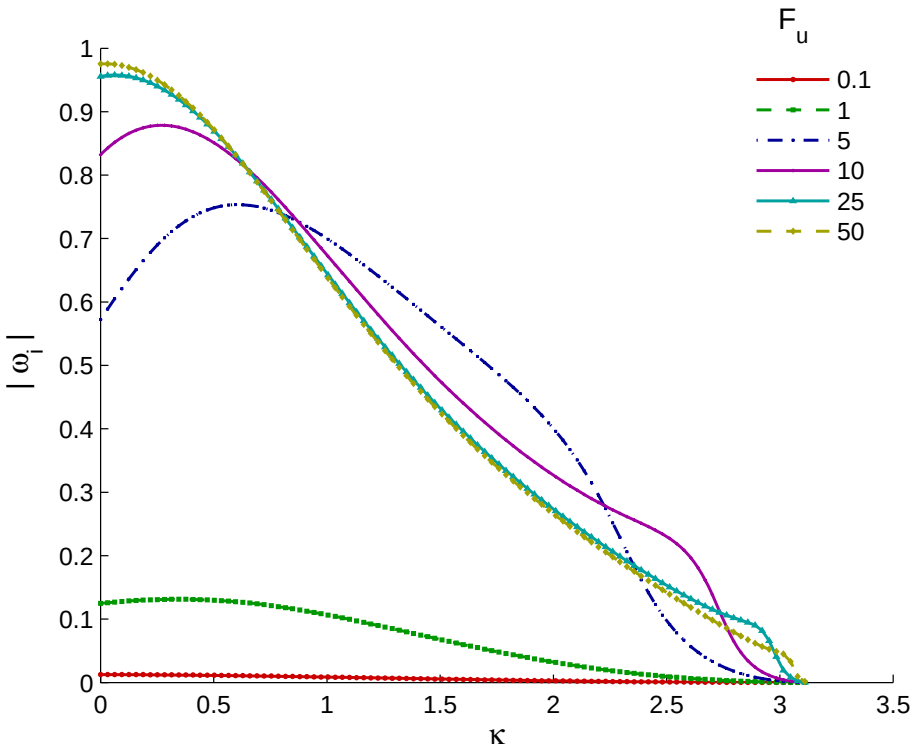

Figure 11: A depiction of the variables used by the een scheme in the calculation of qv^* at the u point in the centre of the figure. The een scheme uses the values of v^* at points A - D and the values of q at points 1-6 at this u point.

$$(qv^*)_{i,j+1/2} = \alpha_{i,j+1/2} v^*_{i+1/2,j+1} + \beta_{i,j+1/2} v^*_{i-1/2,j+1} + \gamma_{i,j+1/2} v^*_{i+1/2,j} + \delta_{i,j+1/2} v^*_{i-1/2,j}. \tag{124}$$

The coefficient at each of these velocity points is calculated (see AL equation (4.21)) using values of q at three nearby q points

$$\begin{aligned} \alpha_{i,j+1/2} &= \frac{1}{12}[q_{i+1,j+1} + q_{i,j+1} + q_{i,j}], \\ \beta_{i,j+1/2} &= \frac{1}{12}[q_{i-1,j+1} + q_{i,j+1} + q_{i,j}], \\ \gamma_{i,j+1/2} &= \frac{1}{12}[q_{i-1,j} + q_{i,j} + q_{i,j+1}], \\ \delta_{i,j+1/2} &= \frac{1}{12}[q_{i+1,j} + q_{i,j} + q_{i,j+1}]. \end{aligned} \tag{125}$$

This article is protected by copyright. All rights reserved.

Accepted Article

At point A the first two of these q points used to calculate α are those on either side of point A (at points 1 and 2). The sum of these two contributions at A is hence given by $\overline{q}^{x} v^{*}/6$ and the sum of the corresponding first two contributions at A, B, C and D is given by

$$C_1 = \frac{2}{3}\overline{(\overline{q}^{x} v^{*})}^{xy} . \tag{126}$$

The other contribution at point A is calculated using the value of q at point 5 in Figure 11a. Point 5 is on the opposite side of the u point from point 2. The remaining contribution at point B also involves q at point 5. So the sum of these two contributions is equal to 1/6 times q at point 5 times $\overline{v^{*}}^{x}$ at point 2. The final remaining contributions from points C and D are given by 1/6 times q at point 2 times $\overline{v^{*}}^{x}$ at point 5. Denoting the "geometric product" for any quantities ϕ and ψ by

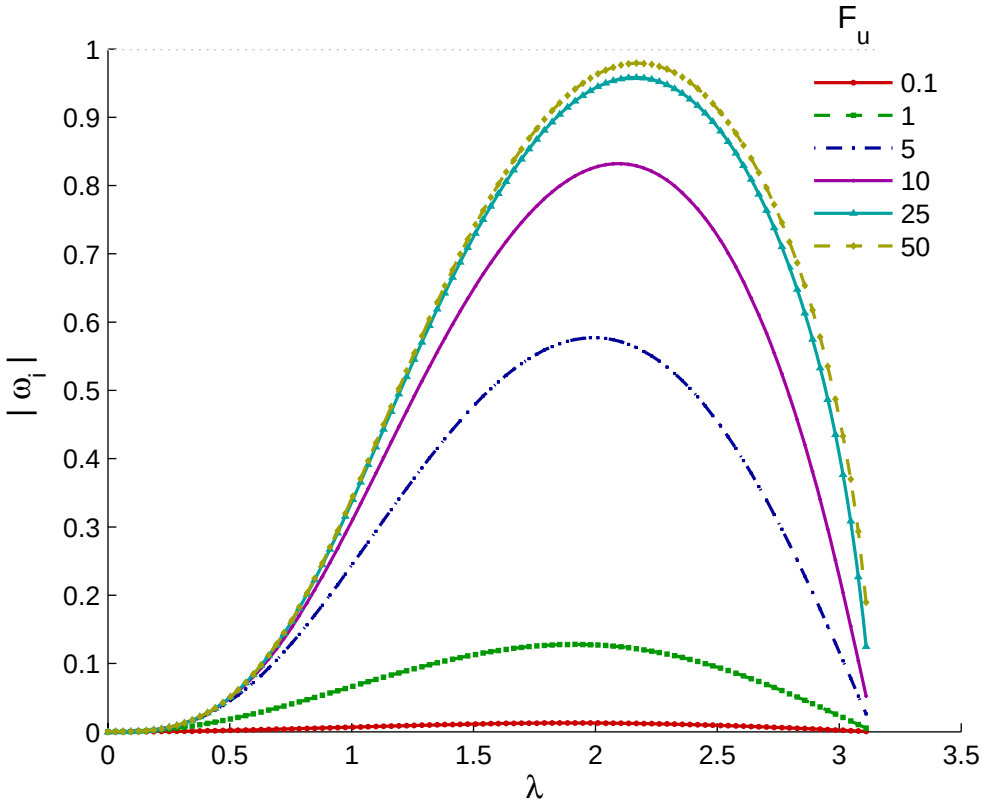

$$G_y(\phi,\psi)_{i,j+1/2} \equiv \frac{1}{2}\left(\phi_{i,j}\psi_{i,j+1} + \phi_{i,j+1}\psi_{i,j}\right), \tag{127}$$

one then sees that the een scheme discretises qv^{*} by

$$(qv^{*})_E = \frac{2}{3}\overline{(\overline{q}^{x} v^{*})}^{xy} + \frac{1}{3} G_y(q, \overline{v^{*}}^{x}). \tag{128}$$

By direct calculation of terms one can establish that

$$G_y(a,b)_{j+1/2} = 2\overline{a}^{y}\overline{b}^{y} - \overline{ab}^{y}. \tag{129}$$

Substituting (129) into (128) one obtains (57a).

This article is protected by copyright. All rights reserved.

Accepted Article

The een scheme calculates qu^* for the u point stored at $(i+1/2, j)$ using

$$\begin{aligned}(qu^*)_{i+1/2,j} = \quad & \gamma_{i+1,j+1/2}u^*_{i+1,j+1/2} + \delta_{i,j+1/2}u^*_{i,j+1/2} \\ + \quad & \alpha_{i,j-1/2}u^*_{i,j-1/2} + \beta_{i+1,j-1/2}u^*_{i+1,j-1/2}.\end{aligned} \tag{130}$$

A similar argument to that given above establishes (57b).

11 Stability analysis for the AL scheme

As for the een scheme the original and modified AL schemes can be concisely written by defining the averaging operators

$$\overline{\psi}^{\mu_A} \equiv \overline{\psi}^{xx}, \quad \overline{\psi}^{\nu_A} \equiv \overline{\psi}^{yy}, \tag{131}$$

where the A subscript indicates the expression is relevant to the AL scheme, and the associated "modified" averaging operators

$$\begin{aligned}\overline{\psi}^{\mu_B} \quad & \equiv \overline{\psi}^{\mu_A}, \quad \overline{\psi}^{\nu_B} \equiv \overline{\psi}^{\nu_A} \quad \text{formodifiedscheme,} \\ \overline{\psi}^{\mu_B} \quad & \equiv \psi, \quad \overline{\psi}^{\nu_B} \equiv \psi \quad \text{fororiginalscheme.}\end{aligned} \tag{132}$$

Similarly to (54) the AL scheme for isopycnal coordinate models sets

$$\eta^{(q)} = \overline{\eta}^{xy}, \quad \eta^{(v)} = \overline{\eta}^{y\mu_B}, \qquad \eta^{(u)} = \overline{\eta}^{x\nu_B}, \tag{133}$$

and discretises the continuity equation as

$$\frac{\partial \eta}{\partial t} + \delta_x\left(\overline{\eta}^{x\nu_B}u\right) + \delta_y\left(\overline{\eta}^{y\mu_B}v\right) = 0. \tag{134}$$

It then discretises the terms qv^* and qu^* in (30) using

$$\begin{aligned}(qv^*)_A = \quad & \overline{(\overline{q}^{xy}\overline{v^*}^{y})}^{x} + \frac{1}{48}\delta_i\left[\left(\delta_i\delta_j q\right)\left(\delta_j v^*\right)\right] \\ & + \delta_i\left(\varepsilon\overline{u^*}^{x}\right) + \overline{\varepsilon\delta_i u^*}^{x},\end{aligned} \tag{135}$$

$$\begin{aligned}(qu^*)_A = \quad & \overline{(\overline{q}^{xy}\overline{u^*}^{x})}^{y} + \frac{1}{48}\delta_j\left[\left(\delta_i\delta_j q\right)\left(\delta_i u^*\right)\right] \\ & + \delta_j\left(\phi\overline{v^*}^{y}\right) + \overline{\phi\delta_j v^*}^{y},\end{aligned} \tag{136}$$

in which (50d) defines δ_i and δ_j and

$$\varepsilon = \frac{1}{12}\delta_j\overline{q}^{x}, \quad \phi = \frac{1}{12}\delta_i\overline{q}^{y}. \tag{137}$$

[Ketefian and Jacobson(2009)] note that the AL scheme can be expressed in the form given by (135) - (136) and these equations are derived in detail in the appendices of [Ketefian(2006)]. For height coordinates the same expressions apply with q replaced by Z, u^* by u and v^* by v.

The original version of the AL scheme takes K_e to be discretised in the same way as in the original een scheme. AL propose a modified form for the kinetic energy in their equation (6.1). A form which is more similar to that used above for the een scheme whose first term gives the same gradients of K_A as the form proposed by AL is given by

This article is protected by copyright. All rights reserved.

Accepted Article

$$2K_A = \overline{u^2}^{xv_B} + \overline{v^2}^{yu_B} - \frac{1}{12}\delta_i\delta_j\left(\overline{u}^{yy}\overline{v}^{xx}\right). \tag{138}$$

The last term in (138) is only used in the modified scheme. It has been introduced here to cancel contributions arising from the Coriolis terms proportional to ε and ϕ in (135) and (136).

Using the above discretisations one finds that in place of (61) - (62) one obtains

$$\begin{aligned}&\frac{\partial u'}{\partial t} - f_0\overline{v'}^{xy} + g\delta_x\eta' + u_1\delta_x\overline{u'}^{xv_B} + v_1\delta_y\overline{u'}^{yu_A}\\ &-\frac{1}{12}\left(u_1\delta_y\delta_i\delta_j\overline{u'}^{u_A} + \delta_B v_1\delta_x\delta_i\delta_j\overline{u'}^{v_A}\right)\\ &+v_1\delta_x\left(\overline{v'}^{yu_B} - \overline{v'}^{yu_A}\right) + \frac{(1-\delta_B)}{12}u_1\delta_x\delta_i\delta_j\overline{v'}^{u_A}\\ &-\delta_I\frac{f_0v_1}{H}\left(\overline{\overline{\eta'}^{u_B} - \overline{\eta'}^{u_A}}\right)^{xyy} = 0,\end{aligned} \tag{139}$$

$$\begin{aligned}&\frac{\partial v'}{\partial t} + f_0\overline{u'}^{xy} + g\delta_y\eta' + u_1\delta_x\overline{v'}^{xv_A} + v_1\delta_y\overline{v'}^{yu_B}\\ &-\frac{1}{12}\left(\delta_B u_1\delta_y\delta_i\delta_j\overline{v'}^{u_A} + v_1\delta_x\delta_i\delta_j\overline{v'}^{v_A}\right)\\ &+u_1\delta_y\left(\overline{u'}^{xv_B} - \overline{u'}^{xv_A}\right) + \frac{(1-\delta_B)}{12}v_1\delta_y\delta_i\delta_j\overline{u'}^{v_A}\\ &+\delta_I\frac{f_0u_1}{H}\left(\overline{\overline{\eta'}^{v_B} - \overline{\eta'}^{v_A}}\right)^{xxy} = 0,\end{aligned} \tag{140}$$

$$\frac{\partial\eta'}{\partial t} + u_1\delta_x\overline{\eta'}^{xv_B} + v_1\delta_y\overline{\eta'}^{yu_B} + H\left(\delta_x u' + \delta_y v'\right) = 0, \tag{141}$$

where

$$\delta_B = 0 \quad \text{for the original scheme,} \quad 1 \quad \text{for the modified scheme.} \tag{142}$$

The first lines of (139) and (140) consist of terms corresponding to those in the original equations. For the modified schemes the other terms are either zero or contribute only to diagonal terms of the stability matrix, so the stability matrix is Hermitian as it was for the een scheme.

12 An interpretation of the stability of the original scheme in isopycnal coordinates

Some insight into why the rather asymmetric matrix obtained for the original schemes in isopycnal coordinates (see (77)) has such simple solutions can be obtained by considering the potential vorticity of the flow and its perturbations. AL show that both the een and AL schemes will not change q in a flow that has uniform q. So one might anticipate that only perturbations whose potential vorticity is identically zero will be able to grow and that this will constrain the instabilities. The calculations presented below support this interpretation.

The linearized form of the potential vorticity (22) is given by

$$q' = \frac{\zeta'}{H} - \overline{\eta'}^{xy}\frac{f_0}{H^2}, \tag{143}$$

and hence, for wave-like solutions,

This article is protected by copyright. All rights reserved.

Accepted Article

$$q_E = \frac{2\mathrm{i}s_\kappa}{H\Delta x}v_E - \frac{2\mathrm{i}s_\lambda}{H\Delta y}u_E - \frac{c_\kappa c_\lambda f_0}{cH}\left(\frac{c\eta_E}{H}\right), \tag{144}$$

where q_E is defined by analogy with (63). Using (144) one sees that the first two rows of (77) can be written as

$$\begin{aligned} \varpi u_E - \mathrm{i}c_\kappa c_\lambda v_E - R_c\frac{s_\kappa}{X}\frac{c\eta_E}{H} + \frac{\mathrm{i}}{2}T_v H\Delta y q_E = 0, \\ \mathrm{i}c_\kappa c_\lambda u_E + \varpi v_E - R_c s_\lambda\frac{c\eta_E}{H} - \frac{\mathrm{i}}{2}T_u H\Delta x q_E = 0. \end{aligned} \tag{145}$$

In other words, the asymmetric terms in the matrix in (77) are proportional to q_E. For perturbations with $q_E = 0$, (77) consequently simplifies to

$$\begin{bmatrix} \varpi & -\mathrm{i}c_\kappa c_\lambda & -\dfrac{R_c s_\kappa}{X} \\ \mathrm{i}c_\kappa c_\lambda & \varpi & -R_c s_\lambda \\ -\dfrac{R_c s_\kappa}{X} & -R_c s_\lambda & \varpi \end{bmatrix}\begin{bmatrix} u_E \\ v_E \\ \dfrac{c\eta_E}{H} \end{bmatrix} = 0. \tag{146}$$

Hence ϖ is the eigenvalue of an Hermitian matrix and is real-valued. So the solutions with $q_E = 0$ are neutrally stable. Moreover, because $q_E = 0$ implies a constraint relating u_E, v_E and η_E, the system (146) has a redundancy, which allows us to drop the third row of equation (146) and use the constraint to eliminate η_E from the first two rows of (146). This reduces (146) to a 2×2 matrix equation

$$\begin{bmatrix} \varpi + A\dfrac{s_\kappa s_\lambda}{\Delta x\Delta y} & -\mathrm{i}c_\kappa c_\lambda - A\dfrac{s_\kappa^2}{\Delta x^2} \\ \mathrm{i}c_\kappa c_\lambda + A\dfrac{s_\lambda^2}{\Delta y^2} & \varpi - A\dfrac{s_\kappa s_\lambda}{\Delta x\Delta y} \end{bmatrix}\begin{bmatrix} u_E \\ v_E \end{bmatrix} = 0. \tag{147}$$

where $A = 4\mathrm{i}c^2/(c_\kappa c_\lambda f_0^2)$. Setting the determinant to zero gives the numerical inertia-gravity wave dispersion relation

$$\varpi^2 = (c_\kappa c_\lambda)^2 + \frac{4c^2}{f_0^2}\left(\frac{s_\kappa^2}{\Delta x^2} + \frac{s_\lambda^2}{\Delta y^2}\right), \tag{148}$$

in agreement with the roots $\varpi^2 = Q^2$ given by (81b) and (82).

The dispersion relation for perturbations in which q_E is non-zero can be determined by using (145) to form a vorticity equation. Multiplying (145b) by $2\mathrm{i}s_\kappa(H\Delta x)^{-1}$ and subtracting $2\mathrm{i}s_\lambda(H\Delta y)^{-1}$ times (145a) one obtains

$$\begin{aligned} \varpi\left(\frac{2\mathrm{i}s_\kappa}{H\Delta x}v_E - \frac{2\mathrm{i}s_\lambda}{H\Delta y}u_E\right) - \frac{2c_\kappa c_\lambda}{H}\left(\frac{s_\kappa}{\Delta x}u_E + \frac{s_\lambda}{\Delta y}v_E\right) \\ + (T_u s_\kappa + T_v s_\lambda)q_E = 0. \end{aligned} \tag{149}$$

Subtracting $c_\kappa c_\lambda f_0(cH)^{-1}$ times the last row of (77) one finds that

$$(\varpi + T_u s_\kappa + T_v s_\lambda)q_E = 0. \tag{150}$$

The factor in parentheses in (150) can vanish only if ϖ is real confirming that wave-like solutions with non-zero potential vorticity are neutrally stable. Note that this factor agrees with

This article is protected by copyright. All rights reserved.

the factor $\varpi + P$ in (82).

Accepted Article

References urlstyle

Adcroft A, Hill C, Marshall J. 1997. Representation of topography by shaved cells in a height coordinate ocean model. *Mon Weather Rev.* **125**: 2293–2315.

Arakawa A, Lamb VR. 1981. A potential enstrophy and energy conserving scheme for the shallow water equations. *Mon. Weather Rev.* **109**: 18–36.

Arakawa A, Mechoso CR, Konor CS. 1992. An isentropic vertical coordinate model: Design and applicaton to atmospheric frontogenesis studies. *Meteor. Atmos. Phys.* **50,1**: 31–45.

Arakawa A, Moorthi S. 1988. Baroclinic instability in vertically discrete systems. *J. Atmos. Sci.* **45**: 1688–1708, doi: http://dx.doi.org/10.1175/1520–0469(1988)045<1688:BIIVDS>2.0.CO;2.

Arakawa A. 2000. A personal perspective on the early years of general circulation modeling at ucla. In: *General circulation model development*, Randall DA (ed), International Geophysics Series, 70, Academic Press, pp. 1–65.

Burridge DM, Haseler JC. 1977. A model for medium range weather forecasting. *ECMWF Tech. Report* **4**.

Daley R. 1988. The normal modes of the spherical non-hydrostatic equations with applications to the filtering of acoustic modes. *Tellus* **40A**: 96–106.

Gassmann A. 2011. Inspection of hexagonal and triangular c-grid discretizations of the shallow water equations. *J. Comput. Phys.* **230**(7): 2706–2721.

Gassmann A. 2013. A global hexagonal C-grid non-hydrostatic dynamical core (ICON-IAP) designed for energetic consistency. *Quart. J. Roy. Meteorol. Soc.* **139**: 152–175.

Gill AE. 1982. *Atmosphere-ocean dynamics*. Academic Press.

Girard C, Plante A, Desgagné M, McTaggart-Cowan R, Côté J, Charron M, Gravel S, Lee V, Patoine A, Qaddouri A, Roch M, Spacek L, Tanguay M, Vaillancourt PA, Zadra A. 2014. Staggered vertical discretization of the canadian environmental multiscale (gem) model using a coordinate of the log-hydrostatic-pressure type. *Mon. Weath. Rev.* **142,3**: 1183–1196, http://dx.doi.org/10.1175/MWR–D–13–00 255.1.

Hollingsworth A, Kallberg P, Renner V, Burridge DM. 1983. An internal symmetric computational instability. *Quart. J. Roy. Meteor. Soc.* **109**: 417–428.

This article is protected by copyright. All rights reserved.

Accepted Article

Ketefian GS, Jacobson MZ. 2009. A mass, energy, vorticity and potential enstrophy and energy conserving lateral fluid-land boundary scheme for the shallow water equations. *J. Comp. Phys.* **228**: 1–32.

Ketefian GS. 2006. *Development and testing of a 2-D potential enstrophy conserving numerical ocean model and a 3-D potential enstrophy conserving non-hydrostatic compressible numerical atmospheric model*. Ph D thesis, Stanford University, http://web.stanford.edu/ gsk/.

Lazi c′ J, Janji c′ Z, Mesinger F. 1986. Non-cancellation instability in horizontal advection schemes for momentum equations. *Meteor. Atmos. Phys.* **35, 1**: 49–52.

Pedlosky J. 1987. *Geophysical Fluid Dynamics*. Springer-Verlag.

Ringler TD, Thuburn J, Klemp JB, Skamarock WC. 2010. A unified approach to energy conservation and potential vorticity dynamics for arbitrarily-structured C-grids. *J. Comp. Phys.* **229**: 3065–3090.

Sadourny R. 1975. The dynamics of finite-difference models of the shallow water equations. *J. Atmos. Sci.* **32**: 680–689.

Skamarock WC, Klemp JB, Duda MG, Fowler LD, Park SH, Ringler TD. 2012. A multiscale nonhydrostatic atmospheric model using centroidal Voronoi tesselations and C-grid staggering. *Mon. Weath. Rev.* **140**: 3090–3105.

Thuburn J, Woollings TJ. 2005. Vertical discretizations for compressible euler equation atmospheric models giving optimal representation of normal modes. *J. Comp. Phys.* **203**: 386–404.

Thuburn J. 2008. Numerical wave propagation on the hexagonal C-grid. *J. Comp. Phys.* **227**: 5836–5858.

Tokioka T. 1978. Some considerations on vertical differencing. *J. Met. Soc. Jap.* **56**: 98–111.

Vallis GK. 2006. *Atmospheric and oceanic fluid dynamics*. Cambridge University Press.

This article is protected by copyright. All rights reserved.